Chapter 1

General Introduction

"Perovskite Chemistry: Synthesis and Application"

Highlights: This chapter discourses on detailed introduction on different types of perovskite materials. Synthetic techniques of these materials and their utility as sensors and photocatalysts are emphasized.

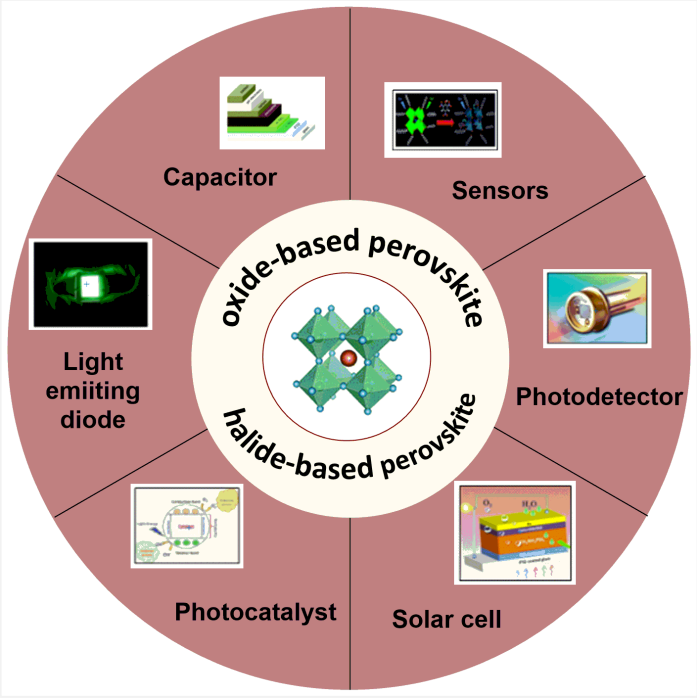

1.1 Introduction to Perovskite Materials

In the 21st century, material chemistry plays an inevitable role in every aspect of human life and civilization. Interest and applications of material chemistry have been growing, and many new branches of this chemistry have been evolving to provide important materials that are simple, efficient, and eco-friendly. Perovskite chemistry is one of the emerging research fields in material chemistry. Though it is primarily known for promising light-harvesting materials, and highly versatile semiconductor sources since the 19th century, these materials are highly relevant to its many applications in concurrent time too. The term perovskite was generally used to designate a special group of crystals that have a distinct orthorhombic, cubic-shaped structure. They have a crystal structure like the naturally occurring mineral $CaTiO_3$. They are comprised of the chemical formula ABX_3 (A^{+2}, B^{+4}, X^{-2}), where A and B are cations and X are anions that bond with both cations [1]. The perovskites featured an impressive array of unique physical properties such as a high absorption coefficient, tuneable bandgap, longer carrier diffusion length, and have gained much attention for their usefulness in light-emitting diodes (LED), photodetectors, catalysis, sensors, fuel cell, etc [2-15]. Because of their specific characteristics, perovskite materials offer a combined property of both organic and inorganic semiconductors.

1.1.1 Brief review of the history of perovskites

Though hybrid perovskite materials are more popular than other types and it has been widely explored in recent times, the very first perovskite material (Calcium Titanate, $CaTiO_3$) was rationalized in the 19th century. German mineralogist Gustav Rose discovered $CaTiO_3$ in the Ural Mountains, located in Russia in the year 1839 [16]. Later, the word perovskite was used to describe the materials having the same crystal structure as we noticed in $CaTiO_3$ (Figure 1.1a). Perovskite materials are found abundantly in nature. Among them, another most abundant perovskite material is magnesium silicate perovskite ($MgSiO_3$) [17]. In the early research phase of perovskite chemistry, oxide-based perovskites were mostly discovered. In 1958, the first halide-based perovskites Cesium Lead Halide ($CsPbX_3$) was revealed (Figure 1.1b). In the year 1970, another halide perovskite Methylammonium halide perovskite was discovered. The importance of halide-based perovskite is quite

remarkable due to their improved electrical and optical properties than early-developed oxide-based perovskites. Later, in 2009, Kojima and co-workers pioneered the first organometal halide perovskites and the research group applied it as a visible photosensitizer in the dye-sensitized solar cell [18]. The same group is known for the first application of perovskite material as a perovskite-sensitized solar cell. As research on solar cell chemistry is another important field, significant research has been carried out to boost the current conversion efficiencies by improving the processing methods and stability of the halide perovskites [19]. In 2014, the first nanocrystal perovskite material $CH_3NH_3PbBr_3$ was realized by Julia and co-workers (Figure 1.1c) [20]. The current research trends with perovskite materials are focused on its wide range of applications, and synthetic methods to improve their stability.

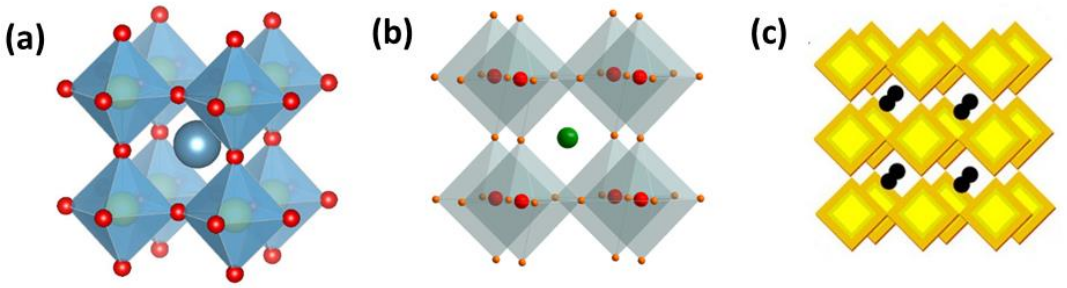

Figure 1.1 Crystal structure of perovskites(a) $CaTiO_3$, (b) $CsPbX_3$, and (c) $CH_3NH_3PbBr_3$

1.1.2 Perovskite Crystal Structure and Tolerance Factor

The perovskite lattice structure is comprised of the chemical formula ABX_3, with A and B being cations and X being halide. In an ideal cubic crystal structure, the B cation is surrounded by six halogen atoms forming a BX_6 octahedral framework, whereas the cation A occupies 12-fold co-ordinated holes with BX_6 octahedra occupying corners and thereby, forms a 3-Dimensional structure (Figure 1.2) [21]. In the ideal cubic perovskite lattice, cation A occupies the cube centre with position (0, 0, 0), cation B occupies the body centre with position (1/2, 1/2, 1/2) and anion X occupies the face-cantered with position (1/2, 1/2, 0). In 1920, Goldsmith introduced the tolerance factor as one of the basic parameters to characterize perovskite materials [22]. The tolerance factor of the crystal is the association between the ionic radii of

the cations and structural geometry. It was calculated by using the following equation [1]:

$$\text{Tolerance factor (t)} = \frac{r_A + r_X}{\sqrt{2}\,(r_B + r_X)} \qquad \ldots [1]$$

In this equation, r_A defines radius of cation A, r_B is radius of cation B and r_x is radius of the halide ion. In the case of an ideal cubic lattice of perovskite structure, the value of the tolerance factor is generally equal to 1. The deviation of t from 1 to a higher or lower value leads to some structural distortions from cubic to rhombohedral, orthorhombic, triclinic, or monoclinic crystal structures, etc [22,23]. Therefore, it is clearly understood that distortions reduce the crystal symmetry by retaining chemical formula. As effect of these distortions can able to reduce the coordination of an A cation from 12 to 8.

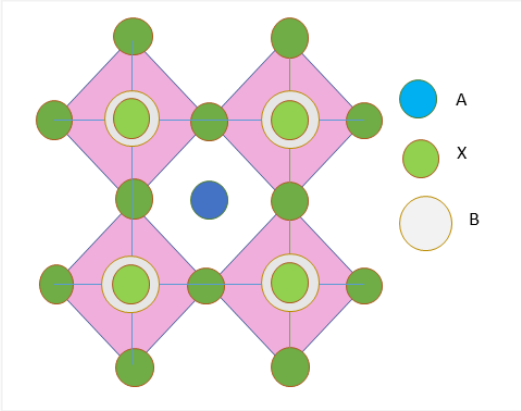

Figure 1.2 Crystal structure of ABX_3 perovskites

1.2 Classification of perovskite crystals

In general, the perovskite family is classified based on their compositions (Figure 1.3). Due to the structural flexibility of the perovskite crystal ABX_3, the crystal structure of perovskite can accommodate a wide range of cations with different oxidation states. Therefore, there are many possibilities for substitutions in the cationic position of the perovskite. Traditionally, based on the nature of the anionic component the perovskite compounds are classified into two categories:

i) Inorganic Oxide perovskite,

ii) Halide perovskite.

Further, halide perovskite is classified into two different types based on its components. The two types are:

a) Inorganic halide perovskite,

b) Organic-inorganic halide perovskite.

1.2.1 Oxide-based Perovskite material: The structural formula for oxide-based perovskites is ABO_3. In this crystal structure, larger cation A occupies with 12-fold coordination and the smaller cation B occupies with 6-fold coordination. Some layered or defective structures also exist in the family of perovskite oxide-based materials. For example, double perovskite structures $A_2B_2X_{5+\delta}$ [24,25] and Ruddlesden–Popper-series $A_{n+1}B_nX_{3n+1}$[26]. The various physiochemical properties such as magnetic, electric, and optical properties can be achieved by the incorporation of different cations in the A and B sites. This type of oxide-based perovskites generally comprises large band gaps and therefore, based on that they exhibit a wide range of electronic and magnetic properties [27]. Oxide-perovskite materials for example $Ca_3Cu_2Ti_4O_{12}$ [28], and $LaMnO_3$ [29] were used as a photocatalyst and capacitors.

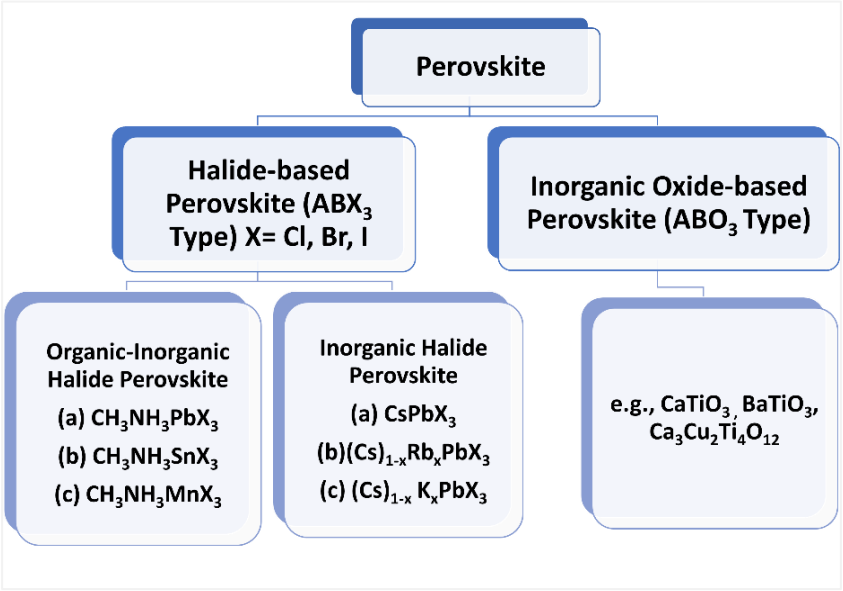

Figure 1.3 Classification of perovskite materials

1.2.2 Halide-based Perovskite materials: The advantage of using halide-based perovskite material is simple and low-cost preparative method, and has excellent properties like their high light absorption, and high charge carrier mobilities [30,31]. The tunability of band gaps of the halide perovskite can be obtained by changing the halide ions or replacing the Pb^{2+} cation with another cation such as Sn^{2+} [32]. Moreover, this type of perovskite is easily stabilized when the tolerance factor ranges

between 0.76 to 1.13 [33]. In the present research era, halide-based perovskites have much potential to show interesting applications because of their intriguing properties such as high quantum yield, high light absorption abilities, etc.

1.2.2.1 Inorganic halide Perovskite: In inorganic halide perovskite materials, the cationic part A is commonly alkali metals such as Cs^+, Li^+, K^+, etc. [32] and the B site possesses cation-like Pb^{2+}, Sn^{2+} or Ge^{2+}, etc [34]. In general, inorganic halide perovskites are more stable than organic-inorganic halide perovskites. They have much potential to be explored as inefficient and commercial devices. Compared to organic-inorganic halide perovskites, the inorganic halide perovskites are more stable against heat. It is studied that methylamine gas (MA) sublimes at 80 ℃ from the perovskite $MAPbI_3$ whereas inorganic halide perovskite is processed at 250-300 ℃ with enhanced crystallinity [35,36].

1.2.2.2 Organic-Inorganic halide Perovskite: In this perovskite, the cationic site A is the organic ammonium cation, and the B site is the divalent cation (Pb^{2+}, Sn^{2+}, Mn^{2+}, Cd^{2+}, etc) [37,38]. The first organic inorganic halide hybrid perovskite, $MAPbI_3$ was discovered by Weber in 1978 [40]. This class of perovskites possesses a band gap tuning, strong optical absorption, high charge carrier mobilities, etc. [38]. However, their instabilities against photo, humidity, and temperature inhibit them to extend their applications in large-scale commercialization. In presence of humidity, the organic cations escape from the cage of Pb-X in the perovskite structure [39].

1.3 Classification based on Stoichiometric Aspects

Based on cationic vacancies, the perovskites can be classified into the following classifications (Figure 1.4):

1.3.1 Tetragonal Perovskites: $BaTiO_3$ is an example of tetragonal perovskites, where the TiO_6 octahedra are somehow distorted in the perovskite lattice [41]. Examples of other tetragonal perovskites are $SrTiO_3$ [42], $CsPbBr_3$ [43], $AgTaO_3$ [44], etc. Due to the presence of distortion, most of them are tetragonal only at high temperatures. So, it is very difficult to study their crystallographic properties at normal temperatures [44].

1.3.2 Rhombohedral Perovskites: In cubic perovskite, small deformation from cubic cells leads to rhombohedral perovskites. The deformation of the rhombohedral angle is either a little less than 90° or less than 60°. Examples of rhombohedral perovskites are $LaAlO_3$ or $LaCoO_3$ etc. This type of perovskite occupies an interesting domain in material chemistry due to its ferroelectric properties [45].

1.3.3 Orthorhombic Perovskites: In an ideal cubic perovskite (ABO_3), the cation A is surrounded by 12 equidistant neighbouring oxygen ions. However, in the case of orthorhombic perovskites, the twelve A–O bonds have four long A–O bond distances and eight short A–O bond distances. In the lattice, the octahedra are rotated or tilted to fill the extra space of the A site [46]. Examples of this type are $GdFeO_3$, $LaRuO_3$, $CaRuO_3$, etc.

1.3.4 Monoclinic and Triclinic Perovskites: Examples of perovskite having monoclinic unit cells are $CsPbI_3$, $BiFeO_3$, $PbSnO_3$, etc. and triclinic unit cell perovskites are $BiScO_3$, $BiMnO_3$ [47-51], etc. They are also known as pseudo cubic unit cell perovskites.

1.3.5 Polymorphism in Perovskites: A great number of oxide-based perovskites and halide-based perovskites undergo polymorphism, and in that process, the structural transitions of the material occur. Metal halide perovskites undergo polymorphic transitions from higher symmetry cubic structures to lower symmetry tetragonal and orthorhombic structures with changing temperature and pressure [52]. However, these phase changes are reversible. All polymorphism perovskites can be called as pseudo cubic perovskites [53]. Examples of this class are $FASnI_3$, $NaBiTiO_3$, etc [54].

1.3.6 Defect Perovskites: In an ideal crystal lattice of perovskites ABX_3/ABO_3, the A cation locates with 12-fold coordination around BX_6 octahedra. All the atoms are in equilibrium positions without any distortions in ideal perovskite. However, in the real scenario, the crystal coordination is not perfect as expected. The cationic, halide/oxide deficiency defects can arise in perovskite materials and create some non-radiative recombination [55]. In the oxide-based perovskite, like, sodium bismuth titanate ($NaBiTiO_3$), there is an increase of oxide-ion conductivity with the formation of defects in the perovskite lattice [56]. Similarly, in the case of pseudo-

cubic perovskite like calcium copper titanate ($CaCu_3Ti_4O_{12}$) too, after the creation of defects in the system, the material exhibits better photocatalytic properties [57]. Moreover, perovskite $LaFeO_3$ with the introduction of calcium (Ca) dopant and oxygen vacancies, the resultant perovskite shows enhanced electrical conductivity [58].

1.3.7 Anti-Perovskites: A perovskite-type structure is found in some semiconductor materials with the structural formula X_3AB. In this case, A and B are anions and X is a cation. In material chemistry, this type of perovskite demonstrates its importance in material chemistry owing to its peculiar properties of charge-discharge capacity, photoluminescence, and ferroelectricity. Examples are Ca_3PN, Sr_3SnO, Ca_3AsN, etc [59].

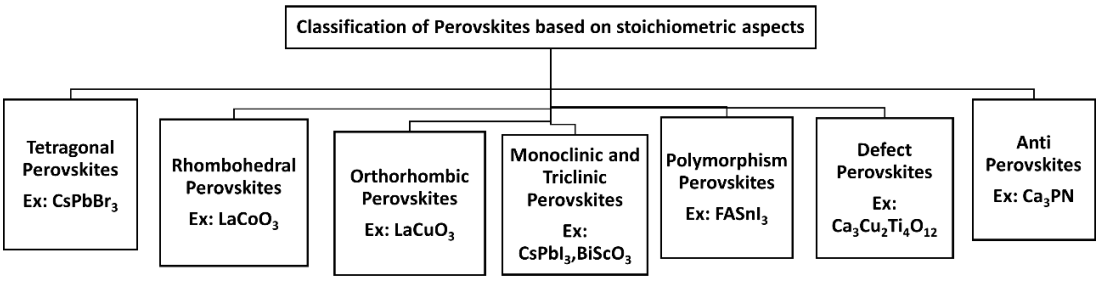

Figure 1.4 Classification based on stoichiometric ratios

1.4 General Properties of Perovskite Materials

The oxide and halide-based perovskites feature several interesting properties like magnetic, conductivity, fluorescence, and catalytic. In this section, a brief note of those benign properties of perovskites is mentioned.

1.4.1 Magnetic properties: The studies of the magnetic properties of perovskite materials bring a new dimension to its applicability. The oxide-based perovskites demonstrate significant magnetic properties due to their strong electron-electron interactions of 3d electrons [60]. Structural flexibilities are common in perovskite structures. The cation B can be replaced with another cation with a suitable oxidation state including main group d-block elements and f-block elements of the periodic table. The double perovskite $A_2B'B''X_3$ shows a good magnetic property because of the presence of paramagnetic cations in the cation site of the crystal structure. Moreover, ferromagnetic, ferrimagnetic, and antiferromagnetic properties are also

commonly observed in perovskite compounds. The ferromagnetic properties arise due to the parallel orientation of magnetic moments resulting in higher magnetic moments, whereas the antiferromagnetic properties exhibit due to the opposite orientation of magnetic moments [61]. The magnetic properties of perovskites can be varied from paramagnetic to anti-ferromagnetic of different temperatures [62]. Some examples of perovskite with excellent magnetic properties are $BiFeO_3$, $ErCrO_3$, etc [62,63].

1.4.2 Electrical properties: Perovskite materials exhibit a range of electrical behaviour ranging from metallic conductors to insulators. Due to the electrical resistivity of the perovskite materials, they can be used as dielectric materials. These materials possess ambipolar charge carrier transport properties and thereby, longer carrier lifetimes. The halide-based perovskite material ($MAPBI_3$) exhibits more than 1μM diffusion length and lifetimes characterized by more than hundreds of nanoseconds [64]. In addition, they have high-charge carrier collection and transport properties. The non-radioactive recombination processes are less in halide-based perovskites. Due to these interesting electrical properties, the materials serve as an efficient electron transport layer in optoelectronic devices.

1.4.3 Optical properties: Perovskite chemistry, a hot topic in concurrent research studies is not only due to their achievement in solar cells, but also their application as light-emitting diodes [65,66] or detectors [67,68]. They have very specific properties like high light absorption coefficient and easily tuneable band gap. In general, major types of perovskites are observed in the cubic, tetragonal, or orthorhombic structure. But in the crystal structure of ABX_3, if the size of cation A reduces, then symmetry changes from tetragonal to cubic [69]. These kinds of symmetry differences contribute to inducing some variations in the band gaps. The band gap for unperturbed $CsPbI_3$ perovskite is 1.67 eV. With the increase in the size of cation A (for example from Cs^+ to MA^+ or FA^+), the band gap of the perturbed perovskite gradually decreases. Similarly, the band gap can also be modified by replacing B cations in ABX_3. Moreover, with the alternation of halide (X) in the perovskite crystal structure, a noticeable change in band gaps is observed. The optical properties of low-dimensional (2D) (nanowire or Quantum dots) are different from the high-dimensional (3D) crystal structure (Figure 1.5). Analogously, 2D

perovskites or quantum perovskites show variable absorption and luminescence properties. In addition, the 2D perovskites are more photostable than the 3D perovskites [70]. In the current trend, the 2D/3D hybrid perovskites are highly applicable as it provides the most desirable optoelectronic properties with improved stabilities [71].

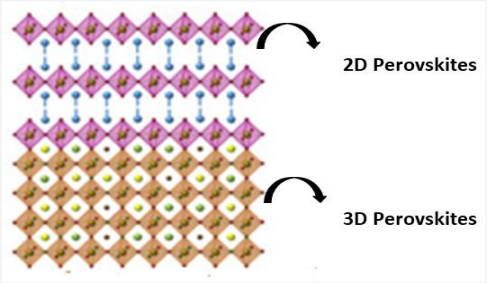

Figure 1.5 Schematic illustration of the 2D/3D perovskites

Moreover, the halide-based perovskites exhibit noticeable optical properties of a wide-colour spectrum with the scope of adjustment for different ranges of colours (from ultraviolet to near-infrared) (Figure 1.6)**.** This basis, with modification of the composition of A cation and X anion, makes them applicable for the application as liquid crystal displays (LCD). The emission spectra of a colloidal dispersion of the perovskite $CsPbX_3$ (where, X = Cl, Br, I, or mixed halide) can be altered over the spectral visible region by adjusting the halide ions [72]. In addition, the quantum confinement effects give a new way to tune the emission properties of halide-based perovskites, which is an important property for light-emitting applications [72]. The luminescence intensity of perovskite is a temperature-dependent property. In $CsPbX_3$ nanocrystals, the intensity gradually quenches with the increment of temperature from 293 K to 373 K [72].

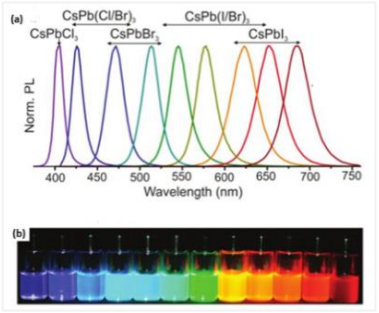

Figure 1.6 a) Emission spectra of $CsPbX_3$ colloidal solution in toluene upon excitation at 365 nm (λ_{ex} = 400 nm for all, but 350 nm for $CsPbCl_3$); b) digital photographs of the respective dispersions upon irradiation with a UV lamp (λ = 365 nm)

1.5 Preparative methods of Perovskite Materials

1.5.1 Synthesis of Perovskite metal-oxides

Perovskite metal oxides are employed in various applications for their extraordinary chemical and physical properties. Different synthetic routes of oxides-based perovskites are described below (Figure 1.7).

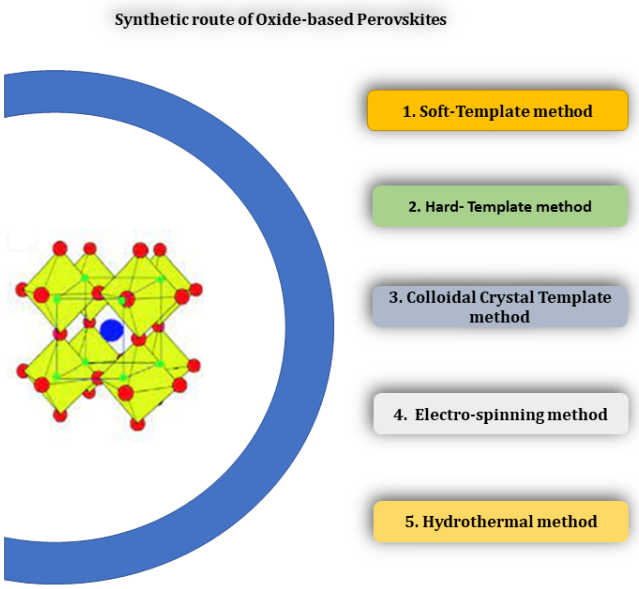

Figure 1.7 Schematic representation of the preparative methods for oxide-based perovskite materials

1.5.1.1 Soft-template method: In the soft-template method, a charged surfactant or a block co-polymer is used, and later the template is removed through the calcination process [73]. However, the method has some issues with the heterogeneity of the cations which leads to the formation of some secondary phases. In a recent development, some chelating agents (urea, citric acid) are used during the preparation of oxide-based perovskites. Formation of homogeneous precursor solutions is occurred due to the addition of these chelating agents, which makes this method better for cation dispersion. Lee and co-workers reported the synthesis of perovskite $La_{0.8}Sr_{0.2}CrO_{3-\delta}$ (δ indicates oxygen deficiency) using this technique using solvent (ethylene glycol, 2- Methoxy ethanol) and using chelating ligand (citric acid, ethylene diamine tetra acetic acid) [74].

1.5.1.2 Hard-template method: In this method to load the metal, mesoporous silica/carbon is used as a template where the template can be further removed through the calcination or acid and alkaline etching processes [75]. Due to the interaction of metal precursors with silica, the removal process of the template is very difficult sometimes. Another problem is that the size of the perovskites is too big for the mesoporous silica. The solution to this issue is the surface functionalization of silica to enhance the impregnation due to the interaction of functional groups with the metal precursors [76]. For example, $LaB_{1-x}B'_xO_3$(B, B' = Mn, Co, Fe, Ni) was synthesized using citric acid as a chelating agent into the metal nitrate with mesoporous silica [77].

1.5.1.3 Colloidal-Crystal template method: The perovskite materials can be synthesized through the colloidal synthesis method. In this method, some organic polymer poly methyl methacrylate (PMMA) [78], and polystyrene (PS) [79] are used. The synthesized perovskites possess sizes ranging from nanometres to micrometres. During the post-synthesis of perovskite materials, the 3D templates are removed by the calcination process at high temperatures. Through this method, the perovskites are prepared with an ordered nano-porous structure. For example, Zhao and co-workers prepared oxide-based perovskite $LaCo_xFe_{1-x}O_3$ by this method using a chelating agent (polyethylene glycol) and some surfactant (citric acid) [80]. This method has some drawbacks like higher time-consuming and high-cost.

1.5.1.4 Electrospinning method: The electrospinning method is another synthetic route to obtain the perovskites with the shape of nanofibers. In this method, a high-voltage electric field is used with an electrostatically driven polymer fluid. The method has applications as the synthesized perovskites are good choices for sensors, catalysis, or optoelectronic devices. During the preparation step, metal nitrates or polymers are used as precursor solutions and the addition of polymer is crucial. Shim and co-workers mentioned the preparatory method of $LaCoO_3$ using this method and later, the material was used in the reduction and evolution of oxygen in rechargeable Zn-air batteries [81].

1.5.1.5 Hydrothermal method: The perovskites prepared through the hydrothermal method have some advantages as this method provides an easy preparative method, high yield, good crystallinity, and low consumption energy [82].

Many oxide-based titanate perovskites like $SrTiO_3$, $CaTiO_3$, etc. can be prepared through this method [83].

1.5.2 Synthesis of Metal-Halide Perovskite

Among the different types of perovskites, metal-halide perovskites (MHPs) represent many new prospects for a research study that ultimately provide potential applications in a wide variety of fields. Different preparative methods of (MHPs) are discussed below (Figure 1.8).

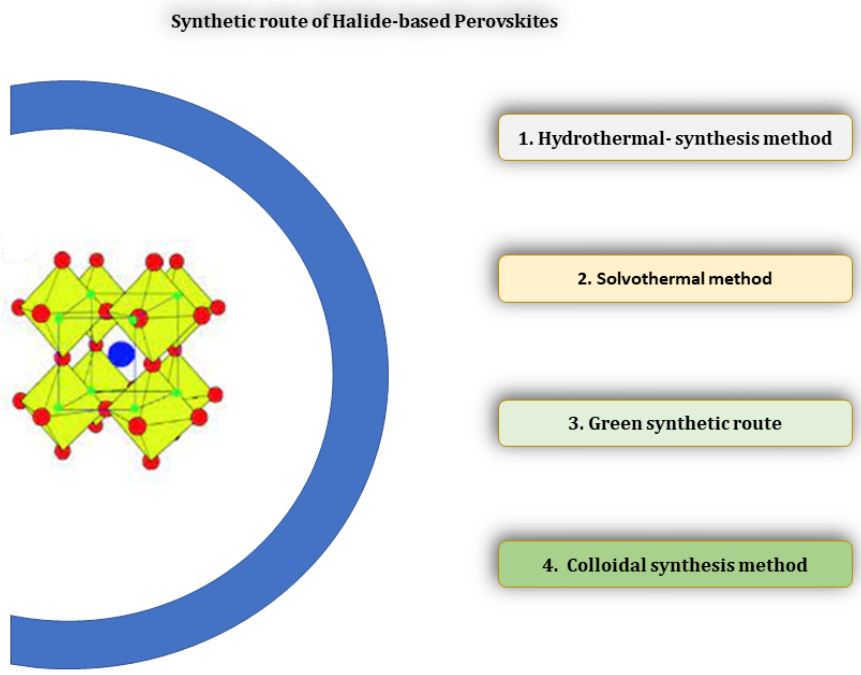

Figure 1.8 Schematic representation of the Preparative methods for halide-based perovskite materials

1.5.2.1 Hydrothermal method: Hydrothermal method is one of the easiest methods to synthesize MHPs. The perovskites prepared using this method deliver the characteristics of high crystallinity. The condition for the reaction for this method is mild under a specific solvent system and the reaction condition does not require high temperature. Therefore, the energy consumption during this preparation method is comparatively low than the other methods. For example, Xia and co-workers synthesized $CH_3NH_3PbI_3$ and $CH_3NH_3PbBr_3$ perovskites in an autoclave at 150 °C using the hydrothermal method, and the material was applied to Li-ion batteries [84]. The perovskites act as a photoelectrode in the Li-ion batteries which can able to

harvest solar energy in the batteries resulting the better current and capacitance values.

1.5.2.2 Solvothermal method: In the solvothermal method, the precursor and the non-aqueous solvents are mixed and kept in a stainless autoclave for a certain period. The obtained product in this method has advantages such as high crystallinity, uniform morphology, etc. Chen and co-workers prepared $CsPbBr_3$ perovskites using the solvothermal method. The product has a high quantum yield (80%) with a narrow full-width half maximum (FWHM) (12-30 nm). Subsequently, the research group used the synthesized perovskites in the light-emitting diodes (LED) [85].

1.5.2.3 Greener Synthetic Route for Metal-Halide Perovskite

1.5.2.3.1 Ultra-sound assisted synthesis method: An ultrasound-assisted method was reported using CH_3NH_3I and PbI_2 as a precursor and the solvent used was isopropanol. The prepared perovskites had a size range of 10-40 nm [86].

1.5.2.3.2 Microwave-assisted synthesis method: In a two-step synthesis process, it is difficult to control the nucleation and crystallization of perovskites. The crystallization process depends on parameters such as humidity, solvent, etc. However, using a thermal annealing process, it is possible to control the properties of the materials. Among other reported methods, the microwave-assisted method is one of the most useful methods. The microwave-assisted method requires a material with appropriate ionic conductivity and dipolar polarization. $MAPbI_3$ perovskites were prepared by applying this method with precursors MAI/PbI_2 and solvent DMF/DMSO [87-88].

1.5.2.3.3 Mechano-synthesis process: This process is an environmental-benign approach where easily accessible mortar and pestle are required. However, different types of milling processes are used in concurrent periods. Stoumpos and co-workers reported the synthesis of halide perovskites, $MAPbI_3$ using the mechano-synthesis method [89].

1.5.2.3.4 Colloidal synthesis method: Among the many synthetic routes for metal-halide perovskites, the colloidal synthesis method is one of the most reliable methods. The synthesized perovskites using this method provide better stability, higher quantum yield, and high crystallinity. This method can be classified into the

top-down approach or bottom-up approach [90]. In the top-down approach, the perovskites are prepared through fragmentation either mechanically or chemically. On the other hand, the bottom-up approach starts with either gas phase or liquid phase reactions. The liquid phase reaction is further classified into the hot-injection method and ligand-assisted reprecipitation method. The hot-injection method requires higher temperature system and an inert environment. In the case of the ligand-assisted reprecipitation method, the desired ions reach a state of equilibrium first, and later, they are precipitated by moving the solution into a state of supersaturation [90]. Huo and workers prepared perovskites through a colloidal synthesis method with different sizes ranging from nanotubes to nanowires [91].

1.6 Applications in diverse areas

As mentioned in the above discussion, due to their outstanding properties, these materials have been studied widely in various fields. The important and highly explored applications of perovskites are discussed below (Figure 1.9).

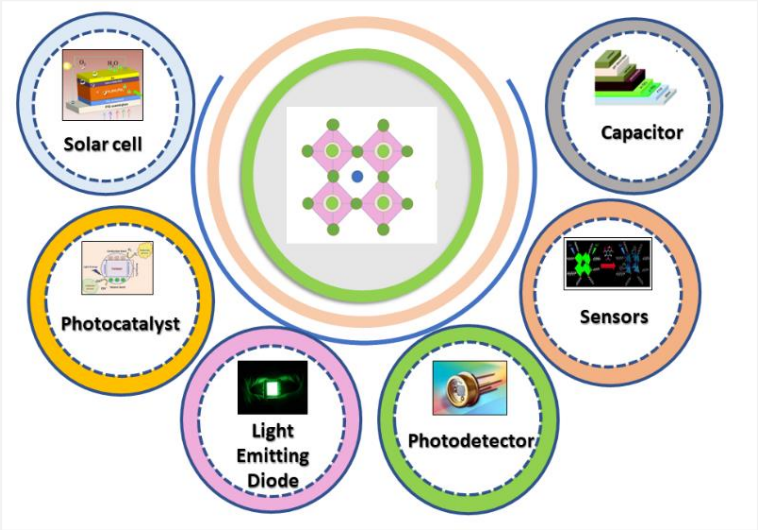

Figure 1.9 Some applications of perovskite-based materials

1.6.1 Solar cell chemistry: Since 2009, perovskite-based solar cells (PSC) disclosed a breakthrough in the solar cell family and become active members. A schematic diagram is shown (Figure 1.10). In the beginning phase, the perovskite materials were applied as a light sensitizer in a dye-sensitized solar cell [18]. In 2011, Park and co-workers, fabricated a perovskite solar cell where TiO_2 acts as an electron transport layer and documented an efficiency of 6.5% [92]. It was reported that perovskite solar cells have better light absorption capacity than dye-sensitized solar

cells. Later in 2011, Gratzel and Seok discovered other perovskite solar cells where the efficiency was 12% [93]. After these initial studies, the importance of perovskite in the solar cell have tremendously investigated and many research groups are working to employ a higher efficiency in perovskite solar cells.

To date, the highest efficiency achieved with the perovskite-based solar cell is 25.2% [94]. Although this material has provided significant advantages, the main drawback of perovskite solar cells is their instability. During the humid condition, the material degrades easily and thereby, making the whole process ineffective. The solar cell is fabricated through the conventional (n-i-p) configuration or the inverted configuration (p-i-n) (n-i-p: FTO/ETL/Perovskite/HTL/Ag).

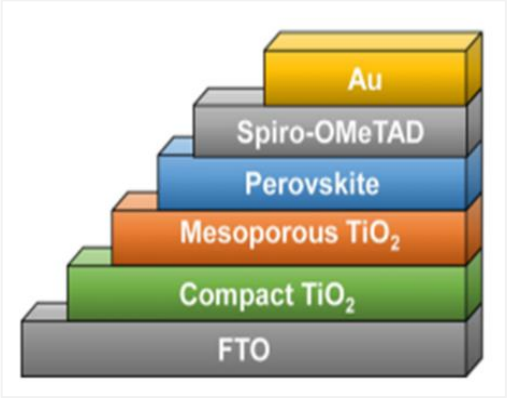

Figure 1.10 Device structure of a perovskite solar cell

1.6.2 Light-emitting diodes: Metal Halide Perovskites (MHPs) are known as a light emitter because of their advancement in high photoluminescence quantum yield (80%), high external quantum efficiency (8%) and current efficiency of 43 cd A^{-1} [95,96] (Figure 1.11). In addition, perovskites have the characteristics of narrow emission, high charge-carrier mobility, colour tunability, etc. However, the intrinsic instability of halide-based perovskites has been identified as a major drawback. In that context, increasing the stability of Perovskite-based light-emitting diodes (PeLED) need further investigation. Replacing the A-site cation with metal Cs^+ or FA^+ is one of the strategies to improve the stability of MHPs. And, suppression of ion migration with additives or blocking layers (ethylene diamine, polyethyleneimine) was reported as an improvement of the stability in PeLED [97].

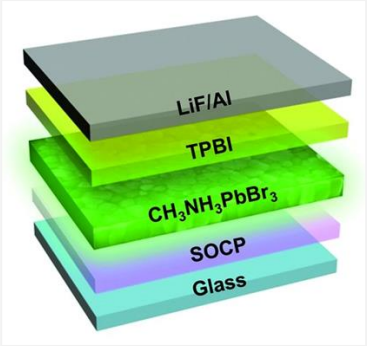

Figure 1.11 Device structure of a Perovskite Light-emitting diode (PeLED).

1.6.3 Perovskite as a Photodetector: As discussed in the early section, halide-based perovskites are known for their significant absorption coefficient, tunable band gap, and long charge carrier diffusion length with high charge mobilities. Due to these specific properties, perovskite-based materials are utilized in broad photodetector applications. Moreover, unlike inorganic substrate Si and Ga, perovskite materials can be fabricated on a flexible substrate which makes them behave as a remarkable photodetector (Figure 1.12). Based on their architecture, the photodetector can be classified into the photovoltaic type and photoconductive type. The photoconductive type detectors are based on the perception of increased electrical conductivity through charge carriers after exposure to light. However, photovoltaic-type detectors can be able to operate even at low temperatures by using light-sensitive materials [98].

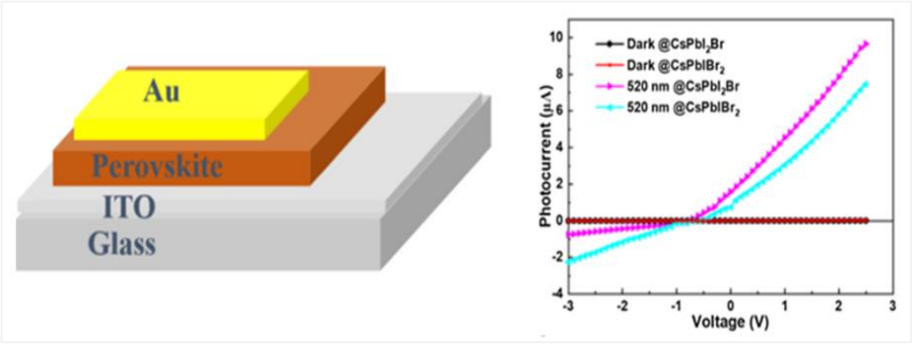

Figure 1.12 Device structure of perovskite-based photodetector with their respective current-voltage characteristics

1.6.4 Perovskite as a supercapacitor: Considering the high-power density, compositional oxygen vacancy, long life cycle, and highly reversible redox capability, the oxide-based perovskites are widely applied in the application of supercapacitors (Figure 1.13). In the crystal structure of perovskite, the replacement of B metal with

another metal or non-metal can boost its performance as a supercapacitor due to the creation of oxygen vacancies [99].

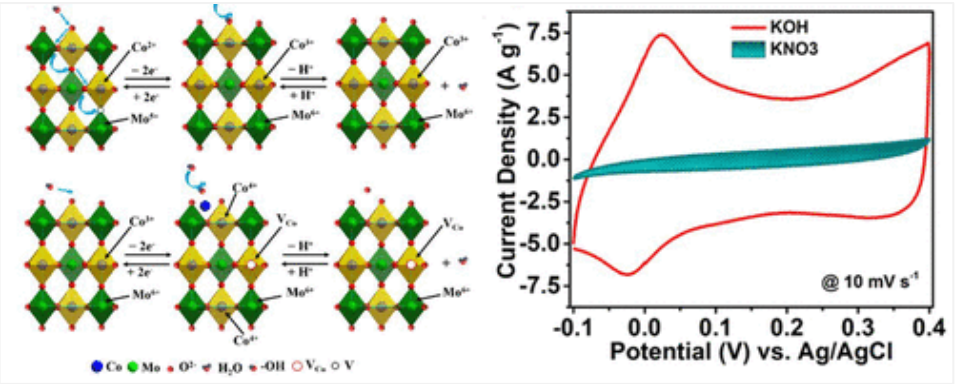

Figure 1.13 Mechanism of oxygen intercalation of the oxide-based perovskites and their respective voltammogram plot [100]

1.6.5 Perovskite as sensors: A sensor device is used to detect the changes in the physical environment upon interaction with the analyte and convert the corresponding changes into readable and reliable signals [101]. Generally, a sensor can be classified into chemical sensors, biosensors, neuromorphic sensors, and metal-oxide-semiconductor sensors. A chemical sensor is composed of two functional units: receptor and transducer. The receptor part interacts with a particular analyte and the transducer part converts the respective physiological and chemical changes into some analytical signals [102]. A biosensor is an analytical device that interacts with biological components such as enzymes, cell receptors, tissue, nucleic acids, antibodies, etc [103]. Neuromorphic sensors are used to detect

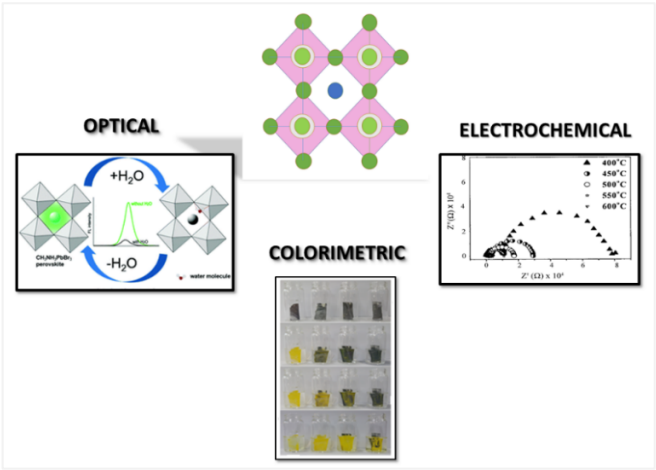

Figure 1.14 Schematic representation of perovskite as sensors

biological neural entities [104]. Several metal-oxide semiconductors (TiO_2, ZnO, etc.) sensors have been utilized to detect analytes [105,106].

The outstanding optical and electrical properties, and flexible structural changes make perovskites a promising candidate for different types of sensing applications (Figure 1.14).

1.6.5.1 Perovskites as an optical sensor: The major disadvantages of organic dye-based sensors are their self-quenching properties, pH dependency, etc. An alternating method for senor probes against organic-dye-based probe is perovskite-based optical sensors. In perovskite-based sensors, when an analyte binds the surface of the perovskite, it causes quenching of its luminescence properties. The interaction mechanisms have been rationalized as Forster resonance energy transfer (FRET), photoinduced electron transfer (PET), recombination, etc. in various studies (Figure 1.15) [12,13]. Generally, in a perovskite crystal structure, the defect states are present in the middle of the valence band and conduction band [107]. The higher quantum yield and the presence of defect states boost perovskite materials as an optical sensor and their application as a probe to detect various analytes.

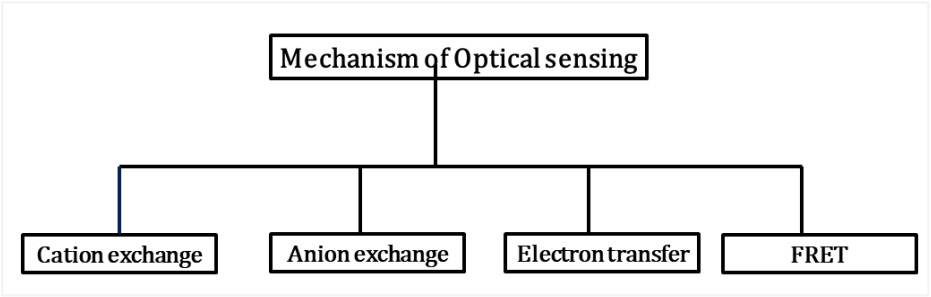

Figure 1.15 Schematic diagram of the mechanism of perovskite as an optical sensor

1.6.5.1.i Cation exchange: When a perovskite compound reacts with an analyte, its cation binds with the B-site of the fluorophores creating some changes to its optical properties (Figure 1.16). Aamir and co-workers synthesized a perovskite material of $CsCuCl_3$ [108]. This perovskite showed a turn-off fluorescence sensor towards metal ions Ag^+ and Hg^+. Also, it displayed a turn-on response towards Pb^{2+}. Another hybrid perovskite $CH_3NH_3PbBr_3$ was applied as a colorimetric fluorescence sensing platform to detect Hg^{2+} [109]. The sensor probe detected cations with a lower detection limit of 0.124 nM (24.87 ppt). Some of the sensing process involves the

replacement of the Pb^{2+} ions by Hg^{2+} ions leading to quenching of the fluorescence peak.

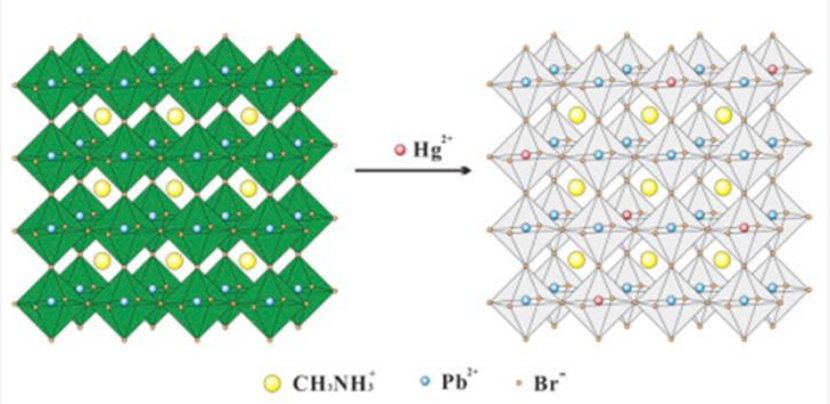

Figure 1.16 Metal cation exchange mechanism

1.6.5.1.ii Anion exchange: In the inorganic perovskite $CsPbBr_3$, their emission wavelength can be altered by exchanging the halide ion (Figure 1.17). Park and co-workers reported a $CsPbBr_3$ combined with cellulose as a colorimetric sensing probe for the detection of chlorine ions. The designed sensor can detect the analyte with a limit of detection of 4.11 nM [110]. Similarly, Dutt and co-workers also prepared $CsPbBr_3$ and used it as an optical sensor through an anion exchange mechanism. The resultant perovskite $CsPbBr_{3-x}Cl_x$ can detect Cl^- ions in an aqueous medium. In their report, there was a specific colour change with the gradual addition of Cl^- ion under UV illumination [111].

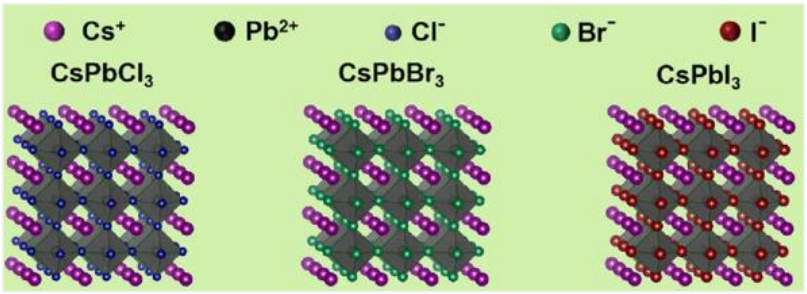

Figure 1.17 Anion exchange mechanism

1.6.5.1.iii Electron transfer mechanism: In perovskite lattice, the arrangement of the valence band of donor and conduction band of acceptor moieties can come with the same alignment. Due to this phenomenon, perovskite materials are compatible with electron transfer between the sensing probe and the analyte. Consequently, some significant changes occur in the physical and chemical properties of the

materials, and the resultant fluctuations help in the detection of analyte (Figure 1.18). In this mechanism, $CsPbBr_3$ perovskites are considered a promising material for sensing applications. The colloidal solution of perovskite was used to detect Cu^{2+} in a non-polar solvent [112]. In the reported perovskite crystal structure, the valence band maxima were dominated by Br^- and the conduction band minima were contributed by Pb^{2+}. With the gradual addition of Cu^{2+} ion, there is the creation of a new state near the valence band maxima of the perovskite crystal structure. Upon excitation, the hole is occupied by this new state. As a result, a non-radiative recombination pathway is responsible for the quenching of the luminescence peak. Ding and co-workers synthesized an eco-friendly non-lead perovskite $Cs_3Bi_2Br_9$. Later, they doped the synthesized perovskite with Eu^{3+} [113]. The new composition $Cs_3Bi_2Br_9$: Eu was applied to detect Cu^{2+} through the electron transfer mechanism. Another example of an electron transfer mechanism was reported by Huang and co-workers [114]. They fabricated a molecularly imprinted polymer (MIP) with $CsPbBr_3$ and applied the material in the detection of omethoate.

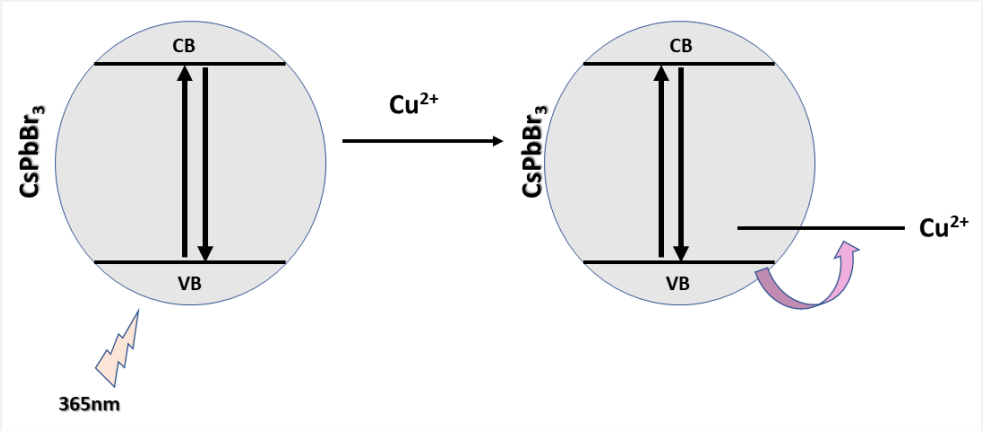

Figure 1.18 Electron transfer mechanism

1.6.5.1.iv Fluorescence resonance electron transfer mechanism (FRET): It is a non-radiative recombination mechanism. During the FRET mechanism, a spectral overlapping takes place between the PL emission spectra of the fluorophore with the UV-Vis absorbance spectra of the acceptor within a distance of 10-100 Å. In this mechanism, the excited donor transfers their energy to an acceptor molecule through the non-radiative process (Figure 1.19). The process depends on the distance between the fluorophore and the analyte. Huang and co-workers synthesized $NH_3(CH_2)_{10}NH_3)PbBr_4$ perovskite and utilized the synthesized material as a sensing

probe for the detection of Hg^{2+} and Rhodamine blue (RhB) [115]. They explained the process that the emission peak of the perovskite overlapped with the absorption spectra of RhB. The calculated distance between the perovskite and RhB was found as 10.37 Å.

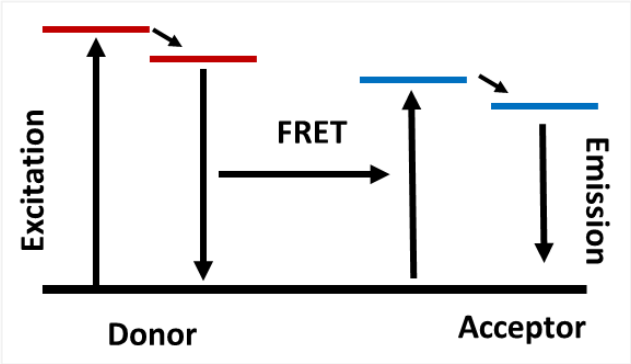

Figure 1.19 FRET mechanism

1.6.5.2 As a colorimetric sensor: Among different types of sensors, the colorimetric sensor is widely recognized due to their benefits like an easily accessible, low-cost, and fast response. With the presence of external stimuli, the colorimetric sensor changes its colour and helps to detect analytes (Figure 1.20). Xu and co-workers reported that when the perovskite $CH_3NH_3PbBr_3$ encountered humidity, a gradual colour change occurred from green to red [116]. The H-bonding interaction between the perovskite and humidity leads to some changes in the crystal structure and this change helps in quenching its emission peak.

Figure 1.20 Photograph showing the different colours of perovskite $CH_3NH_3PbBr_3$ upon exposure to humidity

1.6.5.3 As an electrochemical sensor: Electrochemical sensing platform is another method that delivers a convenient and low-cost detection method to detect the many analytes. It has been widely applied in biomedical and environmental applications. In general, the electrochemical sensing system comprises of three essential parts. A receptor binds with the respective analyte, the specific sample, and then, the transducer part to convert the changes into some readable electrical signal. To report the signals, it has many variables such as voltage, electrochemical impedance, power

output, current, etc [117]. During the detection section, anodic stripping voltammetry (ASV) is commonly used. At first, the analyte is deposited on the electrode where oxidation takes place [118]. The oxide-based perovskite materials where the A site is occupied by alkaline earth metal and B-site is occupied by the transition metals generally show an excellent electrochemical property which is further applied in the catalytic or detection process.

1.6.5.3.i Lanthanide-based perovskite oxide as an electrochemical sensor: Akbari and co-workers developed graphene oxide and $LaMnO_3$ modified glassy carbon electrode [119]. The electrode was further applied in the detection of catechol and hydroquinone using voltametric techniques. In another report, Suvina et al. designed lanthanum cobalt nitrate (LCO)/ hydrotalcite nanotubes (HNT) for the detection of flutamide *via* the electron transfer mechanism. The electrode achieved a limit of detection of 0.002 µM and sensitivity of 0.7571 µA μM^{-1} cm^{-2} [120].

1.6.5.3.ii Strontium-based perovskite oxide as an electrochemical sensor: Mutthukuty et al. synthesized strontium stannate ($SrSnO_3$) and later, prepared $SrSnO_3$-modified glassy carbon as an electrode toward the electrochemical sensing of the anti-inflammatory drug mesalamine (Figure 1.21) [121]. In that report, the lower detection limit was claimed as 0.002 µM.

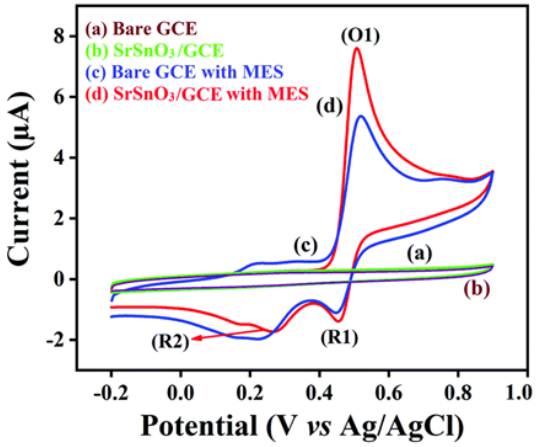

Figure 1.21 $SrSnO_3$ modified glassy carbon for detection of mesalamine

Apart from the detection of antibiotics or drug molecules, perovskite materials have been explored for the detection of various gases such as H_2, H_2S, etc. electrochemically [122,123].

Therefore, from the above discussion, it can be understood that perovskite has great potential as a candidate for sensing purposes. This versatile material provides many scopes to detect temperature, humidity, gas, solvents, metal ions, biomolecules, various explosives, and antibiotics (Figure 1.22).

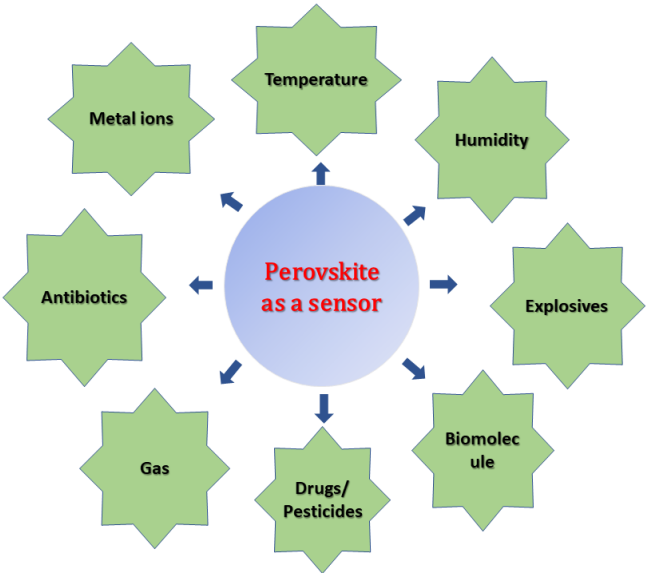

Figure 1.22 Perovskite as a senor towards different analytes

1.6.6 Perovskite as a photocatalyst: A photocatalyst involved with light-induced routes often participates in oxidation-reduction reactions [124]. These redox reactions include water-splitting, toxic-dye degradation, CO_2 reduction, N_2 fixation, etc. In general, the photocatalyst can be classified into three divisions- homogeneous, heterogeneous, and semiconductor. In a homogeneous photocatalyst, the catalyst and the reactant are in the same physical state. On the other hand, in the case of a heterogeneous catalyst, both the reactant and product are in different physical states. However, the semiconductor photocatalyst is excited by the adsorb photon with an energy greater than their band-gap energy, and the generation of electrons and holes is rationalized. The excitons help in the degradation of the studied pollutants and in addition, it is responsible for catalyzing various reactions [124]. The above content can summarise in the following equation:

$$\text{Photocatalyst} + h\nu = \text{Photocatalyst}^* + e^- \text{ (conduction band)} + h^+ \text{ (valence band)} \quad ...(2)$$

In the energy level of the semiconductor, the upper band is known as the conduction band and the lower band is known as the valence band (Figure 1.23). During the transition of excitons, if the two levels are in the same vector, then the transition is

known as direct transition. And, if they are in a different vector, then they are known as indirect transition.

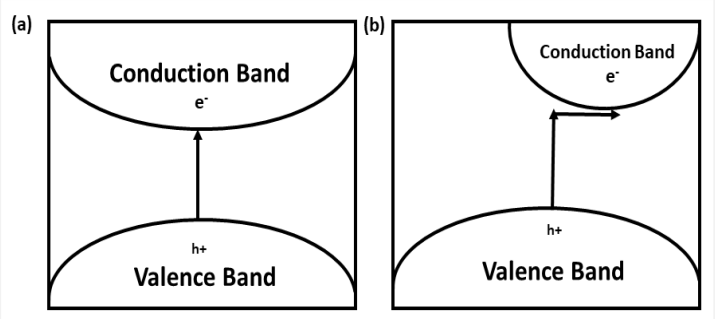

Figure 1.23 Transition in semiconductor; (a) Direct transition, and (b) Indirect transition

Acting as a photocatalyst, the photocatalytic activity of perovskite can be divided into three approaches such as band-gap engineering, suppression of electron-hole pair recombination, and defect engineering. To vary and improve the band gap of the material, the studied techniques are changing its morphology, and creating semiconductor composites. Their photocatalytic applications can be classified into (a) photocatalytic degradation of pollutants, (b) water splitting and hydrogen evaluation, (c) CO_2 reduction, (d) N_2 fixation, and (e) organic transformation (Figure 1.24).

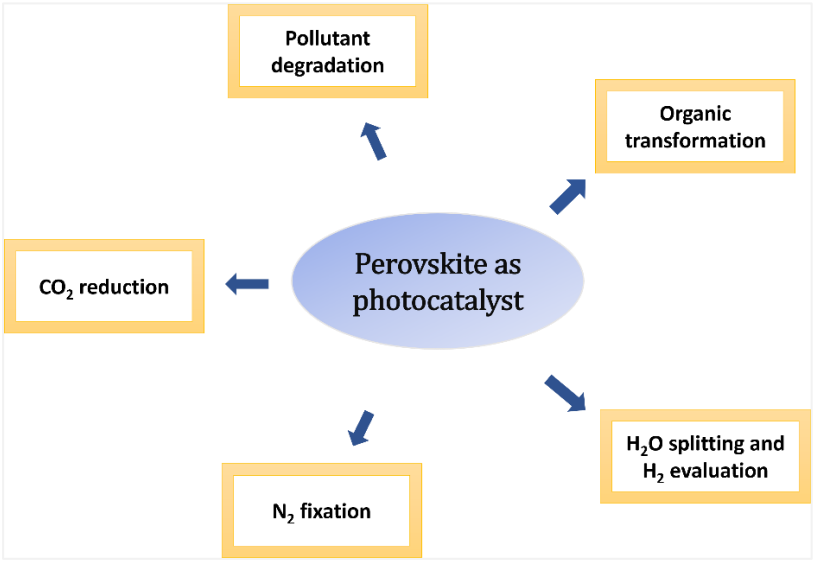

Figure 1.24 Perovskite as a photocatalyst towards different redox reactions

1.6.6.1 Pollutant degradation: With the rapid growth in urbanization and industrialization, the disposal of pollutants is one of the alarming problems and it has

been causing significant damage to our environment. Moreover, many harmful diseases can be seen in humans and becoming a threat to mankind. Degradation of these pollutants is therefore a major concern. With the help of many photocatalysts, it has been possible to degrade those pollutants into some non-harmful molecules. After the generation of excitons in the perovskite materials, they react with the adsorbed species followed by enabling to degrade the toxic molecules into smaller fragments (Figure 1.25). Wang et al. synthesized the perovskite $Ba_4Ti_3O_{12}$ with a band gap of 3.08 eV and applied the material as a photocatalyst for the degradation of methyl-orange dye. In their report, it was found that the photocatalytic performance was enhanced by increasing the annealing temperature [125]. Reitz and co-workers synthesized bismuth ferrite ($BiFeO_3$) in thin film form using poly(ethylene-co-butylene)-block-poly (ethylene oxide) d-block copolymer and the band gap found was 2.9 eV. In that report, the film was applied in the photodegradation of rhodamine blue (RhB) [126]. Like oxide-based perovskites, many metal halide perovskites also have impressive applications for the photodegradation of organic contaminants. In 2019, Morcoso and co-workers published a report on $CsPbBr_3$ quantum dot and used the material in the photodegradation of mercapto-benzothiazole (MBT) [127]. Similarly, Pareez et al. reported $CsSnBr_3$ as a photocatalyst in the photodegradation of crystal violet [128].

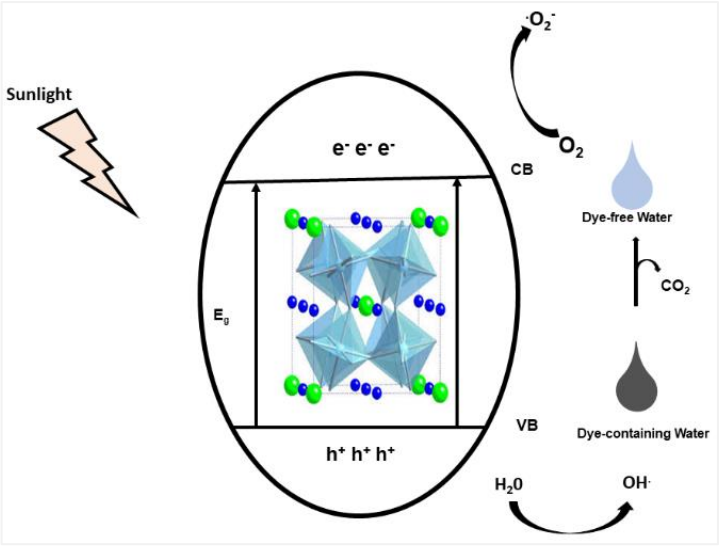

Figure 1.25 Degradation of pollutants by perovskite photocatalyst

1.6.6.2 CO_2 photoreduction: Global warming is a concerning issue; here the increasing level of CO_2 is one of the major contributors. One solution to this problem

is converting CO_2 levels into valuable products. Similar to the plant respiratory process, a suitable photocatalyst might be designed to facilitate CO_2 conversion into some valuable products. In that context, the perovskite photocatalyst is a good candidate for CO_2 photoreduction. In the photoreduction mechanism, the photocatalyst initially adsorbs CO_2, and then, adsorbed light which generates charges on the surface of the photocatalyst (Figure 1.26). The excitons finally help to catalyze the subsequent reactions. End of the reactions, the formed products can be desorbed from the surface of the catalyst. Hou et al. synthesized $CsPbBr_3$ and showed the excellent application of the material in the photoreduction of CO_2 to products such as methane, syngas (CO, CH_4, H_2)[129]. With the yield rate 20.9 µmol/g. Similarly, Kang et al. reported the photocatalytic reduction of $C0_2$ by Au-Cu supported on $SrTiO_3/TiO_2$. In their discussion, the composite produced a heterojunction that subsequently separates their electrons and holes and thus, exhibited better photocatalytic activity.

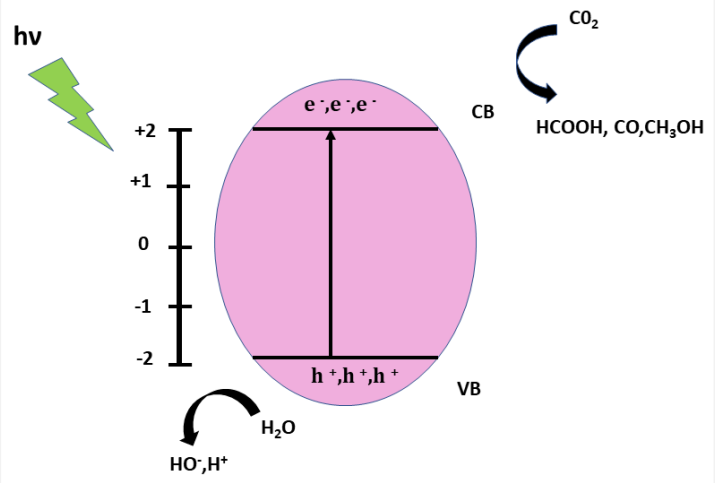

Figure 1.26 Photoreduction of CO_2

1.6.6.3 N_2 fixation: Perovskite materials have been also used in the oxidation and reduction of N_2 fixation. After the generation of electrons and protons by the photocatalyst, N_2 molecules reduce to NH_3. The N_2 molecules react with electrons in the conduction band and the adsorbed water, whereas the holes in the valence band produce H_2O. Finally, the formed NH_3 molecules desorb from the surface of the catalyst. The oxide-based perovskite $BaTiO_3$ effectively converted N_2 into NH_3 with a yield rate of 1.93 $mgL^{-1}h^{-1}$ [131]. Similarly, Song et al. reported La_2TiO_5 perovskite for N_2 fixation with a yield rate of 158.13 $\mu mol.g^{-1}h^{-1}$ [132].

1.6.6.4 H_2O splitting and H_2 evaluation: H_2 evaluation by heterogeneous photocatalysis by using solar energy is a promising way to generate H_2 gas. The opto-electronic properties of perovskite have also been studied to generate H_2 gas. In this domain, Quesada et al. developed a method to develop a stable photocathode for the generation of H_2 gas in water where they used $CH_3NH_3PbI_3$ perovskite encapsulated by InBiSn alloy [133]. Similarly, the oxide-based perovskite ($Nd_{1-x}Co_xFeO_3$) was used in the photocatalytic and photoelectrochemical water-splitting reactions [134].

1.6.6.5 Photocatalytic organic-transformation reaction: With the advancement in the photocatalytic processes, many semiconductor materials have been used as a photocatalyst and they are used for organic transformation reactions. Since perovskite materials possess unique and efficient light-absorbing properties, thus perovskites are too effective photocatalysts in organic-transformation reactions. In this context, Wu et al. used $CsPbBr_3$ perovskites in the reaction of thiol coupling to disulfide conversion and they achieved a yield of 98% [135]. Similarly, $CsPbI_3$ perovskite quantum dots are efficiently used for photocatalytic photopolymerization of 3,4-ethylene-dioxythiophene with a conversion of 32.6% [136].

1.7 Objectives

The perovskite material has been emerged as a promising material for the applications of various opto-electronic devices. However, the degradation under humid conditions is the major drawback of halide-based perovskite. Research has been carried out to improve the stability of halide-based perovskites and to obtain stable perovskite for various applications. The perfect passivation of ligands make perovskite effective towards its applications. The stabilities of halide-based perovskites were improved through the passivation of ligands. Owing to the outstanding luminescence properties of the lead halide perovskite, the halide-based material perovskite is applied as a fluorescence sensor towards solvents and biomolecules. Also, the photocatalytic properties of oxide-based perovskite calcium copper titanate and its application towards dye-degradation of Rhodamine -Blue dye. The objectives of the research work are highlighted below:

- Synthesis of halide and oxide-based perovskites ($CsPbBr_3$ & $Ca_3Cu_2Ti_4O_{12}$) in the bulk and as well as nanoparticles.

- Characterization of the as-synthesized materials using different analytical tools, such as UV-visible Absorbance Spectroscopy, Fourier Transforms Infrared Spectroscopy, Fluorescence spectroscopy, Time-resolved Photoluminescence Spectroscopy, X-ray Diffraction, X-ray photoelectron spectroscopy, Transmission Electron Microscopy, and Scanning Electron Microscopy, etc.
- To optimize the suitable condition to use synthesized perovskite ($CsPbBr_3$) as an effective optical sensor towards different analytes biomolecules such as uric acid, cholesterol and laboratory used solvents such as alcohols .
- Exploration of the photocatalytic performance of the perovskite towards degrading dye.

1.8 Plan of Research-work

To achieve the objectives, the following plan of work will be adopted:

- Synthesis of different passivated and non-passivated perovskites metal halide perovskite Cesium Lead Bromide ($CsPbBr_3$) using one-pot synthesis route.
- Synthesis of oxide-based perovskite Calcium Copper Titanate ($Ca_3Cu_2Ti_4O_{12}$) and its compositions using citrate precursor method.
- Characterization of as-synthesized materials using different analytical tools, such as UV-visible Absorbance Spectroscopy, Fourier Transforms Infrared Spectroscopy, Fluorescence spectroscopy, Time-resolved Photoluminescence Spectroscopy, X-ray Diffraction, X-ray photoelectron spectroscopy, Transmission Electron Microscopy, and Scanning Electron Microscopy, etc.
- Study the stability of the synthesized metal halide perovskites under different conditions.
- Optimization of the suitable condition to using synthesized perovskite ($CsPbBr_3$) as an effective optical sensor towards different analytes.
- Evaluation of the sensing performance for the sensor probe through different analytical tools Stern-Volmer plot, Time-resolved photoluminescence spectra, etc.
- Validation of the sensing performance for practical applications.

- ❖ Exploration of the photocatalytic performance of the oxide-based perovskite calcium copper titanate towards degrading dye using a 20-watt white LED light.
- ❖ Calculation of defect density of the compositions using the deconvoluted method of the respective luminescence spectra.

1.9 Bibliography

[1] Graetzel, M. and Park, N. G. Organometal halide perovskite photovoltaics: a diamond in the rough. *Nano*, 9(05):1440002, 2014.

[2] Yang, X., Zhang, X., Deng, J., Chu, Z., Jiang, Q., Meng, J., Wang, P., Zhang, L., Yin, Z., and You, J. Efficient green light-emitting diodes based on quasi-two-dimensional composition and phase engineered perovskite with surface passivation. *Nature Communications*, 9(1):570, 2018.

[3] Song, T. B., Chen, Q., Zhou, H., Jiang, C., Wang, H. H., Yang, Y. M., Liu, Y., You, J., and Yang, Y. Perovskite solar cells: film formation and properties. *Journal of Materials Chemistry A*, 3(17):9032-9050, 2015.

[4] Song, Z., McElvany, C. L., Phillips, A. B., Celik, I., Krantz, P. W., Watthage, S. C., Liyanage, G. K., Apul, D., and Heben, M. J. A technoeconomic analysis of perovskite solar module manufacturing with low-cost materials and techniques. *Energy & Environmental Science*, 10(6):1297-1305, 2017.

[5] Rong, Y., Liu, L., Mei, A., Li, X., and Han, H. Beyond efficiency: the challenge of stability in mesoscopic perovskite solar cells. *Advanced Energy Materials*, 5(20):1501066, 2015.

[6] Grätzel, M. The rise of highly efficient and stable perovskite solar cells. *Accounts of Chemical Research*, 50(3):487-491, 2017.

[7] Zhang, W., Saliba, M., Stranks, S. D., Sun, Y., Shi, X., Wiesner, U., and Snaith, H. J. Enhancement of perovskite-based solar cells employing core–shell metal nanoparticles. *Nano letters*, 13(9):4505-4510, 2013.

[8] Saliba, M., Stolterfoht, M., Wolff, C. M., Neher, D., and Abate, A. Measuring aging stability of perovskite solar cells. *Joule*, 2(6):1019-1024, 2018.

[9] Hwang, J., Rao, R. R., Giordano, L., Katayama, Y., Yu, Y., and Shao-Horn, Y. Perovskites in catalysis and electrocatalysis. *Science*, 358(6364):751-756, 2017.

[10] Arandiyan, H., Mofarah, S. S., Sorrell, C. C., Doustkhah, E., Sajjadi, B., Hao, D., Wang, Y., Sun, H., Ni, B. J., and Rezaei, M. Defect engineering of oxide perovskites for catalysis and energy storage: synthesis of chemistry and materials science. *Chemical Society Reviews*, 50(18):10116-10211, 2021.

[11] Wang, Y., Chi, Z., Chen, C., Su, C., Liu, D., Liu, Y., Duan, X., and Wang, S. Facet- and defect-dependent activity of perovskites in catalytic evolution of sulfate radicals. *Applied Catalysis B: Environmental*, 272: 118972, 2020.

[12] Zhu, Z., Sun, Q., Zhang, Z., Dai, J., Xing, G., Li, S., Huang, X., and Huang, W. Metal halide perovskites: stability and sensing-ability. *Journal of Materials Chemistry C*, 6(38):10121-10137, 2018.

[13] Halali, V. V., Sanjayan, C., Suvina, V., Sakar, M., and Balakrishna, R. G. Perovskite nanomaterials as optical and electrochemical sensors. *Inorganic Chemistry Frontiers*, 7(14):2702-2725, 2020.

[14] Yu, J., Ran, R., Zhong, Y., Zhou, W., Ni, M., and Shao, Z. Advances in porous perovskites: synthesis and electrocatalytic performance in fuel cells and metal–air batteries. *Energy & Environmental Materials*, 3(2):121-145, 2020.

[15] Tarancón, A., Skinner, S. J., Chater, R. J., Hernandez-Ramirez, F., and Kilner, J. A. Layered perovskites as promising cathodes for intermediate temperature solid oxide fuel cells. *Journal of Materials Chemistry*, 17(30):3175-3181, 2007.

[16] Goldschmidt, V. M. Die gesetze der krystallochemie. *Naturwissenschaften*, 14(21):477-485, 1926.

[17] Hirose, K., Sinmyo, R., and Hernlund, J. Perovskite in Earth's deep interior. *Science*, 358(6364):734-738, 2017.

[18] Kojima, A., Teshima, K., Shirai, Y., and Miyasaka, T. Organometal halide perovskites as visible-light sensitizers for photovoltaic cells. *Journal of the American Chemical Society*, 131(17):6050-6051, 2009.

[19] Im, J. H., Lee, C. R., Lee, J. W., Park, S. W., and Park, N. G. 6.5% efficient perovskite quantum-dot-sensitized solar cell. *Nanoscale*, 3(10):4088-4093, 2011.

[20] Schmidt, L. C., Pertegás, A., González-Carrero, S., Malinkiewicz, O., Agouram, S., Minguez Espallargas, G., Bolink, H. J., Galian, R. E., and Pérez-Prieto, J. Nontemplate synthesis of $CH_3NH_3PbBr_3$ perovskite nanoparticles. *Journal of the American Chemical Society*, 136(3):850-853, 2014.

[21] Lu, C. H., Biesold-McGee, G. V., Liu, Y., Kang, Z., and Lin, Z. Doping, and ion substitution in colloidal metal halide perovskite nanocrystals. *Chemical Society Reviews*, 49(14):4953-5007, 2020.

[22] Bhalla, A., Guo, R., and Roy, R. The perovskite structure: a review of its role in ceramic science and technology. *Materials Research Innovations*, 4(1):3-26, 2000.

[23] Richter, J., Holtappels, P., Graule, T., Nakamura, T., and Gauckler, L. J. Materials design for perovskite SOFC cathodes. *Monatshefte für Chemie-Chemical Monthly*, 140:985-999, 2009.

[24] Kubicek, M., Bork, A. H., and Rupp, J. L. Perovskite oxides: a review on a versatile material class for solar-to-fuel conversion processes. *Journal of Materials Chemistry A*, 5(24):11983-12000, 2017.

[25] Wu, C., Zhang, Q., Liu, Y., Luo, W., Guo, X., Huang, Z., Ting, H., Sun, W., Zhong, X., and Wei, S. The dawn of lead-free perovskite solar cell: highly stable double perovskite $Cs_2AgBiBr_6$ film. *Advanced Science*, 5(3):1700759, 2018.

[26] Tsai, H., Nie, W., Blancon, J. C., Stoumpos, C. C., Asadpour, R., Harutyunyan, B., Neukirch, A. J., Verduzco, R., Crochet, J. J., and Tretiak, S. High-efficiency two-dimensional Ruddlesden–Popper perovskite solar cells. *Nature*, 536(7616):312-316, 2016.

[27] Suntivich, J., Gasteiger, H. A., Yabuuchi, N., Nakanishi, H., Goodenough, J. B., and Shao-Horn, Y. Design principles for oxygen-reduction activity on perovskite oxide catalysts for fuel cells and metal–air batteries. *Nature Chemistry*, 3(7):546-550, 2011.

[28] Kawrani, S., Boulos, M., Cornu, D., and Bechelany, M. From synthesis to applications: copper calcium titanate (CCTO) and its magnetic and photocatalytic properties. *ChemistryOpen*, 8(7):922-950, 2019.

[29] Nagamuthu, S., Vijayakumar, S., and Ryu, K. S. Cerium oxide mixed $LaMnO_3$ nanoparticles as the negative electrode for aqueous asymmetric supercapacitor devices. *Materials Chemistry and Physics*, 199:543-551, 2017.

[30] Sheikh, A. D., Bera, A., Haque, M. A., Rakhi, R. B., Del Gobbo, S., Alshareef, H. N., and Wu, T. Atmospheric effects on the photovoltaic performance of hybrid perovskite solar cells. *Solar Energy Materials and Solar Cells*, 137:6-14, 2015.

[31] Wang, B., Xiao, X., and Chen, T. Perovskite photovoltaics: a high-efficiency newcomer to the solar cell family. *Nanoscale*, 6(21):12287-12297, 2014.

[32] Zhang, Y., Liu, J., Wang, Z., Xue, Y., Ou, Q., Polavarapu, L., Zheng, J., Qi, X., and Bao, Q. Synthesis, properties, and optical applications of low-dimensional perovskites. *Chemical Communications*, 52(94):13637-13655, 2016.

[33] Wang, W., Tade, M. O., and Shao, Z. Research progress of perovskite materials in photocatalysis and photovoltaics-related energy conversion and environmental treatment. *Chemical Society Reviews*, 44(15):5371-5408, 2015.

[34] Tian, J., Xue, Q., Yao, Q., Li, N., Brabec, C. J., and Yip, H. L. Inorganic halide perovskite solar cells: progress and challenges. *Advanced Energy Materials*, 10(23):2000183, 2020.

[35] Juarez-Perez, E. J., Ono, L. K., Maeda, M., Jiang, Y., Hawash, Z., and Qi, Y. Photodecomposition, and thermal decomposition in methylammonium halide lead perovskites and inferred design principles to increase photovoltaic device stability. *Journal of Materials Chemistry A*, 6(20):9604-9612, 2018.

[36] Xiang, W., Wang, Z., Kubicki, D. J., Tress, W., Luo, J., Prochowicz, D., Akin, S., Emsley, L., Zhou, J., and Dietler, G. Europium-doped $CsPbI_2B_r$ for stable and highly efficient inorganic perovskite solar cells. *Joule*, 3(1):205-214, 2019.

[37] Kagan, C. R., Mitzi, D. B., and Dimitrakopoulos, C. D. Organic-inorganic hybrid materials as semiconducting channels in thin-film field-effect transistors. *Science*, 286(5441):945-947, 1999.

[38] Ma, L., Guo, D., Li, M., Wang, C., Zhou, Z., Zhao, X., Zhang, F., Ao, Z., and Nie, Z. Temperature-dependent thermal decomposition pathway of organic–inorganic halide perovskite materials. *Chemistry of Materials*, 31(20):8515-8522, 2019.

[39] Luo, S. and Daoud, W. A. Recent progress in organic–inorganic halide perovskite solar cells: mechanisms and material design. *Journal of Materials Chemistry A*, 3(17):8992-9010, 2015.

[40] Weber, D. $CH_3NH_3SnBr_xI_{3-x}$ (x = 0-3), ein Sn (II) - system mit kubischer perowskitstruktur/$CH_3NH_3SnBr_xI_{3-x}$ (x = 0-3), a Sn (II) - system with cubic perovskite structure. *Zeitschrift für Naturforschung B*, 33(8):862-865, 1978.

[41] Muhsen, K. N. D. K., Osman, R. A. M., and Idris, M. S. The effects of Ca, Zr and Sn substitutions into a ternary system of $BaTiO_3$–$BaSnO_3$–$BaZrO_3$ towards its

dielectric and piezoelectric properties: a review. *Journal of Materials Science: Materials in Electronics*, 32:12771-12783, 2021.

[42] Bian, W., Lu, X., Li, Y., Min, C., Zhu, H., Fu, Z., and Zhang, Q. Influence of Nd doping on microwave dielectric properties of $SrTiO_3$ ceramics. *Journal of Materials Science: Materials in Electronics*, 29:2743-2747, 2018.

[43] Ghaithan, H. M., Alahmed, Z. A., Qaid, S. M., Hezam, M., and Aldwayyan, A. S. Density functional study of cubic, tetragonal, and orthorhombic $CsPbBr_3$ perovskite. *ACS Omega*, 5(13):7468-7480, 2020.

[44] Farid, U., Khan, H. U., Avdeev, M., Injac, S., and Kennedy, B. J. Structural studies of the high temperature phases of $AgTaO_3$. *Journal of Solid State Chemistry*, 258:859-864, 2018.

[45] Megaw, H. D. and Darlington, C. Geometrical and structural relations in the rhombohedral perovskites. *Acta Crystallographica Section A: Crystal Physics, Diffraction, Theoretical and General Crystallography*, 31(2):161-173, 1975.

[46] Kobayashi, H., Nagata, M., Kanno, R., and Kawamoto, Y. Structural characterization of the orthorhombic perovskites: [$ARuO_3$ (A = Ca, Sr, La, Pr)]. *Materials Research Bulletin*, 29(12):1271-1280, 1994.

[47] Yuan, G., Qin, S., Wu, X., Ding, H. and Lu, A. Pressure-induced phase transformation of $CsPbI_3$ by X-ray diffraction and Raman spectroscopy. *Phase Transitions*, 91(1):38-47, 2018.

[48] Cardoso, J. O. P., Delmonte, D., Gilioli, E., Fertman, E. L., Fedorchenko, A. V., Shvartsman, V. V., Paukšta, V., Grigalaitis, R., Banys, J. R., and Khalyavin, D. D. Phase Transitions in the Metastable Perovskite Multiferroics $BiCrO_3$ and $BiCr_{0.9}Sc_{0.1}O_3$: A Comparative Study. *Inorganic Chemistry*, 59(13):8727-8735, 2020.

[49] Xing, X., Chen, J., Wei, G., Deng, J., and Liu, G. Synthesis and stability of nanocrystalline lead stannate. *Journal of the American Ceramic Society*, 87(7):1371-1373, 2004.

[50] Belik, A. A., Iikubo, S., Yokosawa, T., Kodama, K., Igawa, N., Shamoto, S., Azuma, M., Takano, M., Kimoto, K., and Matsui, Y. Origin of the monoclinic-to-monoclinic phase transition and evidence for the centrosymmetric crystal structure of $BiMnO_3$. *Journal of the American Chemical Society*, 129(4):971-977, 2007.

[51] Inaguma, Y., Miyaguchi, A., Yoshida, M., Katsumata, T., Shimojo, Y., Wang, R., and Sekiya, T. High-pressure synthesis, and ferroelectric properties in perovskite-type $BiScO_3$–$PbTiO_3$ solid solution. *Journal of Applied Physics*, 95(1):231-235, 2004.

[52] Alaei, A., Circelli, A., Yuan, Y., Yang, Y., and Lee, S. S. Polymorphism in metal halide perovskites. *Materials Advances*, 2(1):47-63, 2021.

[53] Ozório, M. S., Srikanth, M., Besse, R., and Da Silva, J. L. The role of the A-cations in the polymorphic stability and optoelectronic properties of lead-free $ASnI_3$ perovskites. *Physical Chemistry Chemical Physics*, 23(3):2286-2297, 2021.

[54] Yang, F., Li, M., Li, L., Wu, P., Pradal-Velázque, E., and Sinclair, D. Optimisation of oxide-ion conductivity in acceptor-doped $Na_{0.5}Bi_{0.5}TiO_3$ perovskite: approaching the limit? *Journal of Materials Chemistry A*, 5(41):21658-21662, 2017.

[55] Fu, L., Li, H., Wang, L., Yin, R., Li, B., and Yin, L. Defect passivation strategies in perovskites for an enhanced photovoltaic performance. *Energy & Environmental Science*, 13(11):4017-4056, 2020.

[56] Yang, F., Li, M., Li, L., Wu, P., Pradal-Velázquez, E., and Sinclair, D. Defect chemistry and electrical properties of sodium bismuth titanate perovskite. *Journal of Materials Chemistry A*, 6(13):5243-5254, 2018.

[57] Ahmadipour, M., Arjmand, M., Ahmad, Z. A., and Pung, S. Y. Photocatalytic degradation of organic dye by sol–gel-synthesized $CaCu_3Ti_4O_{12}$ powder. *Journal of Materials Engineering and Performance*, 29:2006-2014, 2020.

[58] Song, J., Zhu, S., Ning, D., and Bouwmeester, H. J. Defect chemistry and transport properties of perovskite-type oxides $La_{1-x}Ca_xFeO_{3-\delta}$. *Journal of Materials Chemistry A*, 9(2):974-989, 2021.

[59] Cheng, H., Mao, A. J., Yang, S. M., Tian, H., Jin, S. Y., Yu, M., and Kuang, X. Y. Semiconductor-to-metal reconstructive phase transition and superconductivity of anti-perovskite Ca_3PN under hydrostatic pressure. *Journal of Materials Chemistry C*, 8(37):13072-13078, 2020.

[60] Mahadevan, P., Shanthi, N., and Sarma, D. Estimates of electronic interaction parameters for $LaMO_3$ compounds (M = Ti–Ni) from ab initio approaches. *Physical Review B*, 54(16):11199, 1996.

[61] Jonker, G. Magnetic compounds with perovskite structure IV Conducting and non-conducting compounds. *Physica*, 22(6-12):707-722, 1956.

[62] Su, Y., Zhang, J., Li, L., Li, B., Zhou, Y., Deng, D., Chen, Z., and Cao, S. Temperature dependence of magnetic properties and change of a specific heat in perovskite $ErCrO_3$ chromites. *Applied Physics A*, 100:73-78, 2010.

[63] Park, T. J., Papaefthymiou, G. C., Viescas, A. J., Moodenbaugh, A. R., and Wong, S. S. Size-dependent magnetic properties of single-crystalline multiferroic $BiFeO_3$ nanoparticles. *Nano Letters*, 7(3):766-772, 2007.

[64] Stranks, S. D., Eperon, G. E., Grancini, G., Menelaou, C., Alcocer, M. J., Leijtens, T., Herz, L. M., Petrozza, A., and Snaith, H. J. Electron-hole diffusion lengths exceeding 1 micrometer in an organometal trihalide perovskite absorber. *Science*, 342(6156):341-344, 2013.

[65] Lin, K., Xing, J., Quan, L. N., de Arquer, F. P. G., Gong, X., Lu, J., Xie, L., Zhao, W., Zhang, D., and Yan, C. Perovskite light-emitting diodes with external quantum efficiency exceeding 20 per cent. *Nature*, 562(7726):245-248, 2018.

[66] Li, H., Lin, H., Ouyang, D., Yao, C., Li, C., Sun, J., Song, Y., Wang, Y., Yan, Y., and Wang, Y. Efficient and Stable Red Perovskite Light-Emitting Diodes with Operational Stability > 300 h. *Advanced Materials*, 33(15):2008820, 2021.

[67] Tian, W., Zhou, H., and Li, L. Hybrid organic–inorganic perovskite photodetectors. *Small*, 13(41):1702107, 2017.

[68] Saidaminov, M. I., Adinolfi, V., Comin, R., Abdelhady, A. L., Peng, W., Dursun, I., Yuan, M., Hoogland, S., Sargent, E. H., and Bakr, O. M. Planar-integrated single-crystalline perovskite photodetectors. *Nature Communications*, 6(1):8724, 2015.

[69] Snaith, H. J. Present status and future prospects of perovskite photovoltaics. *Nature Materials*, 17(5):372-376, 2018.

[70] Leung, T. L., Ahmad, I., Syed, A. A., Ng, A. M. C., Popović, J., and Djurišić, A. B. Stability of 2D and *quasi*-2D perovskite materials and devices. *Communications Materials*, 3(1):63, 2022.

[71] Lee, H. B., Kumar, N., Tyagi, B., Ko, K. J., and Kang, J. W. Dimensionality and defect engineering using fluoroaromatic cations for efficiency and stability enhancement in 3D/2D perovskite photovoltaics. *Solar RRL*, 5(3):2000589, 2021.

[72] He, X., Qiu, Y., and Yang, S. Fully inorganic trihalide perovskite nanocrystals: A new research frontier of optoelectronic materials. *Advanced Materials*, 29(32):1700775, 2017.

[73] Huo, Q., Margolese, D. I., Ciesla, U., Feng, P., Gier, T. E., Sieger, P., Leon, R., Petroff, P. M., Schüth, F., and Stucky, G. D. Generalized synthesis of periodic surfactant/inorganic composite materials. *Nature*, 368(6469):317-321, 1994.

[74] Lee, B. I., Gupta, R. K., and Whang, C. M. Effects of solvent and chelating agent on synthesis of solid oxide fuel cell perovskite, $La_{0.8}Sr_{0.2}CrO_{3-\delta}$. *Materials Research Bulletin*, 43(2):207-221, 2008.

[75] Gu, D. and Schüth, F. Synthesis of non-siliceous mesoporous oxides. *Chemical Society Reviews*, 43(1):313-344, 2014.

[76] Huang, X., Yang, M., Wang, G., and Zhang, X. Effect of surface properties of SBA-15 on confined Ag nanomaterials *via* double solvent technique. *Microporous and Mesoporous Materials*, 144(1-3):171-175, 2011.

[77] De Lima, R., Batista, M., Wallau, M., Sanches, E., Mascarenhas, Y. P., and Urquieta-González, E. A. High specific surface area LaFeCo perovskites—Synthesis by nanocasting and catalytic behaviour in the reduction of NO with CO. *Applied Catalysis B: Environmental*, 90(3-4):441-450, 2009.

[78] Liu, Y., Dai, H., Du, Y., Deng, J., Zhang, L., and Zhao, Z. Lysine-aided PMMA-templating preparation, and high performance of three-dimensionally ordered macro-porous $LaMnO_3$ with mesoporous walls for the catalytic combustion of toluene. *Applied Catalysis B: Environmental*, 119:20-31, 2012.

[79] Sadakane, M., Asanuma, T., Kubo, J., and Ueda, W. Facile procedure to prepare three-dimensionally ordered macroporous (3DOM) perovskite-type mixed metal oxides by colloidal crystal templating method. *Chemistry of Materials*, 17(13):3546-3551, 2005.

[80] Xu, J., Liu, J., Zhao, Z., Zheng, J., Zhang, G., Duan, A., and Jiang, G. Three-dimensionally ordered macroporous $LaCo_xFe_{1-x}O_3$ perovskite-type complex oxide catalysts for diesel soot combustion. *Catalysis Today*, 153(3-4):136-142, 2010.

[81] Shim, J., Lopez, K., Sun, H. J., Park, G., An, J. C., Eom, S., Shimpalee, S., and Weidner, J. Preparation, and characterization of electro-spun $LaCoO_3$ fibres

for oxygen reduction and evolution in rechargeable Zn–air batteries. *Journal of Applied Electrochemistry*, 45:1005-1012, 2015.

[82] Shi, W., Song, S., and Zhang, H. Hydrothermal synthetic strategies of inorganic semiconducting nanostructures. *Chemical Society Reviews*, 42(13):5714-5743, 2013.

[83] Pan, J. H., Shen, C., Ivanova, I., Zhou, N., Wang, X., Tan, W. C., Xu, Q. H., Bahnemann, D. W., and Wang, Q. Self-template synthesis of porous perovskite titanate solid and hollow sub-microspheres for photocatalytic oxygen evolution and mesoscopic solar cells. *ACS Applied Materials & Interfaces*, 7(27):14859-14869, 2015.

[84] Xia, H. R., Sun, W. T., and Peng, L. M. Hydrothermal synthesis of organometal halide perovskites for Li-ion batteries. *Chemical Communications*, 51(72):13787-13790, 2015.

[85] Chen, M., Zou, Y., Wu, L., Pan, Q., Yang, D., Hu, H., Tan, Y., Zhong, Q., Xu, Y., and Liu, H. Solvothermal synthesis of high-quality all-inorganic cesium lead halide perovskite nanocrystals: from nano-cube to ultrathin nanowire. *Advanced Functional Materials*, 27(23):1701121, 2017.

[86] Kumar, V. B., Gouda, L., Porat, Z. E., and Gedanken, A. Sono-chemical synthesis of $CH_3NH_3PbI_3$ perovskite ultrafine nanocrystal sensitizers for solar energy applications. *Ultrasonics Sonochemistry*, 32:54-59, 2016.

[87] Vidyasagar, C., Muñoz Flores, B. M., and Jiménez Pérez, V. M. Recent advances in synthesis and properties of hybrid halide perovskites for photovoltaics. *Nano-Micro Letters*, 10:1-34, 2018.

[88] Guo, Y., Shoyama, K., Sato, W., Matsuo, Y., Inoue, K., Harano, K., Liu, C., Tanaka, H., and Nakamura, E. Chemical pathways connecting lead(II) iodide and perovskite *via* polymeric plumbate(II) fibre. *Journal of the American Chemical Society*, 137(50):15907-15914, 2015.

[89] Stoumpos, C. C., Malliakas, C. D., and Kanatzidis, M. G. Semiconducting tin and lead iodide perovskites with organic cations: phase transitions, high mobilities, and near infrared photoluminescent properties. *Inorganic Chemistry*, 52(15):9019-9038, 2013.

[90] Shamsi, J., Urban, A. S., Imran, M., De Trizio, L., and Manna, L. Metal halide perovskite nanocrystals: synthesis, post-synthesis modifications, and their optical properties. *Chemical Reviews*, 119(5):3296-3348, 2019.

[91] Huo, C., Fong, C. F., Amara, M. R., Huang, Y., Chen, B., Zhang, H., Guo, L., Li, H., Huang, W., and Diederichs, C. Optical spectroscopy of single colloidal $CsPbBr_3$ perovskite nanoplatelets. *Nano Letters*, 20(5):3673-3680, 2020.

[92] Akhil, S., Kusuma, J., Akash, S., and Balakrishna, R. G. Perovskite-like ceramic hole transport material for quantum dot sensitized solar cells. *Solar Energy*, 224:355-360, 2021.

[93] Heo, J. H., Im, S. H., Noh, J. H., Mandal, T. N., Lim, C. S., Chang, J. A., Lee, Y. H., Kim, H. J., Sarkar, A., and Nazeeruddin, M. K. Efficient inorganic–organic hybrid heterojunction solar cells containing perovskite compound and polymeric hole conductors. *Nature Photonics*, 7(6):486-491, 2013.

[94] Zeng, P., Deng, W., and Liu, M. Recent advances of device components toward efficient flexible perovskite solar cells. *Solar RRL*, 4(3): 1900485, 2020.

[95] Veldhuis, S. A., Boix, P. P., Yantara, N., Li, M., Sum, T. C., Mathews, N., and Mhaisalkar, S. G. Perovskite materials for light-emitting diodes and lasers. *Advanced Materials*, 28(32):6804-6834, 2016.

[96] Cho, H., Kim, Y. H., Wolf, C., Lee, H. D., and Lee, T. W. Improving the stability of metal halide perovskite materials and light-emitting diodes. *Advanced Materials*, 30(42):1704587, 2018.

[97] Lee, S., Park, J. H., Lee, B. R., Jung, E. D., Yu, J. C., Di Nuzzo, D., Friend, R. H., and Song, M. H. Amine-based passivating materials for enhanced optical properties and performance of organic–inorganic perovskites in light-emitting diodes. *The Journal of Physical Chemistry Letters*, 8(8):1784-1792, 2017.

[98] Yu, X., Tsao, H. N., Zhang, Z., and Gao, P. Miscellaneous and perspicacious: hybrid halide perovskite materials-based photodetectors and sensors. *Advanced Optical Materials*, 8(21):2001095, 2020.

[99] Cao, Y., Liang, J., Li, X., Yue, L., Liu, Q., Lu, S., Asiri, A. M., Hu, J., Luo, Y., and Sun, X. Recent advances in perovskite oxides as electrode materials for supercapacitors. *Chemical Communications*, 57(19):2343-2355, 2021.

[100] Meng, D., Gu, H., Lu, Q., Zhao, Y., Zhu, G., Zhang, Y., Zhong, Q., and Bu, Y. Advances, and perspectives for the application of perovskite oxides in supercapacitors. *Energy & Fuels*, 35(21):17353-17371, 2021.

[101] Xu, X., Zhou, J., Xin, Y., Lubineau, G., Ma, Q., and Jiang, L. Alcohol recognition by flexible, transparent, and highly sensitive graphene-based thin-film sensors. *Scientific Reports*, 7(1):1-10, 2017.

[102] Thungon, P. D., Kakoti, A., Ngashangva, L., and Goswami, P. Advances in developing rapid, reliable, and portable detection systems for alcohol. *Biosensors and Bioelectronics*, 97:83-99, 2017.

[103] Ates, M. A review study of (bio) sensor systems based on conducting polymers. *Materials Science and Engineering: C*, 33(4):1853-1859, 2013.

[104] Rivera-Acosta, M., Ortega-Cisneros, S., Rivera, J., and Sandoval-Ibarra, F. American sign language alphabet recognition using a neuromorphic sensor and an artificial neural network. *Sensors*, 17(10):2176, 2017.

[105] Zakrzewska, K. and Radecka, M. TiO_2-based nanomaterials for gas sensing-influence of anatase and rutile contributions. *Nanoscale Research Letters*, 12:1-8, 2017.

[106] Bhatia, S., Verma, N., and Bedi, R. Ethanol gas sensor based upon ZnO nanoparticles prepared by different techniques. *Results in Physics*, 7:801-806, 2017.

[107] Zhang, Q., Zheng, W., Wan, Q., Liu, M., Feng, X., Kong, L., and Li, L. Confined Synthesis of Stable and Uniform $CsPbBr_3$ Nanocrystals with High Quantum Yield up to 90% by High Temperature Solid-State Reaction. *Advanced Optical Materials*, 9(11):2002130, 2021.

[108] Aamir, M., Sher, M., Malik, M. A., Akhtar, J., and Revaprasadu, N. A chemodosimetric approach for the selective detection of Pb^{2+} ions using a cesium-based perovskite. *New Journal of Chemistry*, 40(11):9719-9724, 2016.

[109] Lu, L. Q., Tan, T., Tian, X. K., Li, Y., and Deng, P. Visual and sensitive fluorescent sensing for ultra trace mercury ions by perovskite quantum dots. *Analytica Chimica Acta*, 986:109-114, 2017.

[110] Park, B., Kang, S. M., Lee, G. W., Kwak, C. H., Rethinasabapathy, M., and Huh, Y. S. Fabrication of $CsPbBr_3$ perovskite quantum dots/cellulose-based

colorimetric sensor: Dual-responsive on-site detection of chloride and iodide ions. *Industrial & Engineering Chemistry Research*, 59(2):793-801, 2019.

[111] Vasavi Dutt, V., Akhil, S., and Mishra, N. Cesium Lead Bromide Perovskite Nanocrystals as a Simple and Portable Spectrochemical Probe for Rapid Detection of Chlorides. *ChemistrySelect*, 6(31):8171-8176, 2021.

[112] Sheng, X., Liu, Y., Wang, Y., Li, Y., Wang, X., Wang, X., Dai, Z., Bao, J., and Xu, X. Cesium lead halide perovskite quantum dots as a photoluminescence probe for metal ions. *Advanced Materials*, 29(37):1700150, 2017.

[113] Ding, N., Zhou, D., Pan, G., Xu, W., Chen, X., Li, D., Zhang, X., Zhu, J., Ji, Y., and Song, H. Europium-doped lead-free $Cs_3Bi_2Br_9$ perovskite quantum dots and ultrasensitive Cu^{2+} detection. *ACS Sustainable Chemistry & Engineering*, 7(9):8397-8404, 2019.

[114] Huang, S., Guo, M., Tan, J., Geng, Y., Wu, J., Tang, Y., Su, C., Lin, C. C., and Liang, Y. Novel fluorescence sensor based on all-inorganic perovskite quantum dots coated with molecularly imprinted polymers for highly selective and sensitive detection of omethoate. *ACS Applied Materials & Interfaces*, 10(45):39056-39063, 2018.

[115] Huang, Y., Yan, F., Xu, J., Bian, Y., Zhang, R., Wang, J., and Zhou, X. The FRET performance and aggregation-induced emission of two-dimensional organic-inorganic perovskite, and its application to the determination of Hg(II). *Microchimica Acta*, 184:3513-3519, 2017.

[116] Xu, W., Li, F., Cai, Z., Wang, Y., Luo, F., and Chen, X. An ultrasensitive and reversible fluorescence sensor of humidity using perovskite $CH_3NH_3PbBr_3$. *Journal of Materials Chemistry C*, 4(41):9651-9655, 2016.

[117] Baranwal, J., Barse, B., Gatto, G., Broncova, G., and Kumar, A. Electrochemical sensors, and their applications: a review. *Chemosensors*, 10(9):363, 2022.

[118] Guziejewski, D. Square-wave Amplitude Effect in Cathodic and Anodic Stripping Square-wave Voltammetry. *Electroanalysis*, 31(2):231-238, 2019.

[119] Akbari, S., Foroughi, M. M., Nadiki, H. H., and Jahani, S. Synthesis, and characterization of $LaMnO_3$ nanocrystals and graphene oxide: fabrication of graphene oxide–$LaMnO_3$ sensor for simultaneous electrochemical determination of hydroquinone and catechol. *Journal of Electrochemical Science and Engineering*, 9(4):255-267, 2019.

[120] Suvina, V., Kokulnathan, T., Wang, T. J., and Balakrishna, R. G. Unraveling the electrochemical properties of lanthanum cobaltite decorated halloysite nanotube nanocomposite: An advanced electrocatalyst for determination of flutamide in environmental samples. *Ecotoxicology and Environmental Safety*, 190:110098, 2020.

[121] Muthukutty, B., Karthik, R., Chen, S. M., and Abinaya, M. Designing novel perovskite-type strontium stannate ($SrSnO_3$) and its potential as an electrode material for the enhanced sensing of anti-inflammatory drug mesalamine in biological samples. *New Journal of Chemistry*, 43(31):12264-12274, 2019.

[122] Natkaeo, A., Phokharatkul, D., Hodak, J. H., Wisitsoraat, A., and Hodak, S. K. Highly selective sub-10 ppm H_2S gas sensors based on Ag-doped $CaCu_3Ti_4O_{12}$ films. *Sensors and Actuators B: Chemical*, 260:571-580, 2018.

[123] Zhang, H., Yi, J., and Jiang, X. Fast response, highly sensitive and selective mixed-potential H_2 sensor based on (La, Sr)(Cr, Fe)$O_{3-\delta}$ perovskite sensing electrode. *ACS Applied Materials & Interfaces*, 9(20):17218-17225, 2017.

[124] Kushwaha, H., Madhar, N. A., Ilahi, B., Thomas, P., Halder, A., and Vaish, R. Efficient solar energy conversion using $CaCu_3Ti_4O_{12}$ photoanode for photocatalysis and photo-electrocatalysis. *Scientific Reports*, 6(1):18557, 2016.

[125] Yao, W. F., Xu, X. H., Wang, H., Zhou, J. T., Yang, X. N., Zhang, Y., Shang, S. X., and Huang, B. B. Photocatalytic property of perovskite bismuth titanate. *Applied Catalysis B: Environmental*, 52(2):109-116, 2004.

[126] Reitz, C., Suchomski, C., Weidmann, C., and Brezesinski, T. Block copolymer-templated $BiFeO_3$ nanoarchitectures composed of phase-pure crystallites intermingled with a continuous meso-porosity: Effective visible-light photocatalysts. *Nano Research*, 4(4): 414, 2011.

[127] Cardenas-Morcoso, D., Gualdrón-Reyes, A. S. F., Ferreira Vitoreti, A. B., García-Tecedor, M., Yoon, S. J., Solis de la Fuente, M., Mora-Seró, I. N., and Gimenez, S. Photocatalytic and photoelectrochemical degradation of organic compounds with all-inorganic metal halide perovskite quantum dots. *The Journal of Physical Chemistry Letters*, 10(3):630-636, 2019.

[128] Reyes-Pérez, F., Gallardo, J. J., Aguilar, T., Alcántara, R., Fernández-Lorenzo, C., and Navas, J. Visible-light-enhanced photocatalytic activity of totally inorganic halide-based perovskite. *ChemistrySelect*, 3(36):10226-10235, 2018.

[129] Hou, J., Cao, S., Wu, Y., Gao, Z., Liang, F., Sun, Y., Lin, Z., and Sun, L. Inorganic colloidal perovskite quantum dots for robust solar CO_2 reduction. *Chemistry–A European Journal*, 23(40):9481-9485, 2017.

[130] Kang, Q., Wang, T., Li, P., Liu, L., Chang, K., Li, M., and Ye, J. Photocatalytic reduction of carbon dioxide by hydrous hydrazine over Au–Cu alloy nanoparticles supported on $SrTiO_3/TiO_2$ coaxial nanotube arrays. *Angewandte Chemie*, 127(3):855-859, 2015.

[131] Zhao, Z., Wang, D., Gao, R., Wen, G., Feng, M., Song, G., Zhu, J., Luo, D., Tan, H., and Ge, X. Magnetic-field-stimulated efficient photocatalytic N_2 fixation over defective $BaTiO_3$ perovskites. *Angewandte Chemie International Edition*, 60(21):11910-11918, 2021.

[132] Song, M., Wang, L., Li, J., Sun, D., Guan, R., Zhai, H., Gao, X., Li, X., Zhao, Z., and Sun, Z. Defect density modulation of La_2TiO_5: An effective method to suppress electron-hole recombination and improve photocatalytic nitrogen fixation. *Journal of Colloid and Interface Science*, 602:748-755, 2021.

[133] Crespo-Quesada, M., Pazos-Outón, L. M., Warnan, J., Kuehnel, M. F., Friend, R. H., and Reisner, E. Metal-encapsulated organo-lead halide perovskite photocathode for solar-driven hydrogen evolution in water. *Nature Communications*, 7(1):12555, 2016.

[134] Ilanchezhiyan, P., Kumar, G. M., Siva, C., Cho, H., Lee, D., Reddy, N. L., Ramu, A., Kang, T., and Kim, D. Neodymium (Nd) based oxide perovskite nanostructures for photocatalytic and photoelectrochemical water splitting functions. *Environmental Research*, 197:111128, 2021.

[135] Wu, W. B., Wong, Y. C., Tan, Z. K., and Wu, J. Photo-induced thiol coupling and C–H activation using nanocrystalline lead-halide perovskite catalysts. *Catalysis Science & Technology*, 8(16):4257-4263, 2018.

[136] Chen, K., Deng, X., Dodekatos, G., and Tüysüz, H. Photocatalytic polymerization of 3,4-ethylenedioxythiophene over cesium lead iodide perovskite quantum dots. *Journal of the American Chemical Society*, 139(35):12267-12273, 2017.